Delft University of Technology
Bachelor Thesis

Exoplanet surface mapping for Fresnel light curves

Author
Tim Mulder

Supervised by
Dr. Paul M. Visser
Dr. Aurèle J.L. Adam
committee members
Dr. Ir. Wolter Groenevelt
Dr. Akira Endo

Faculty of Electrical Engineering, Mathematics and Computer Science
Faculty of Applied Sciences TU Delft

Nomenclature

A vector is displayed in boldface ($\mathbf{v}$), a unit vector is denoted with a hat ($\hat{\mathbf{v}}$)

r	Radius of the exoplanet
R	Radius of the star
I	Inclination of the solar system
n	THe tilt axis
ω	Orbital angular velocity
Ω	Spin angular velocity
γ	Orbital angle
Γ	Spin angle
$\hat{\mathbf{r}}$	Unit vector from the star pointing to the planet
$\hat{\mathbf{n}}$	Unit vector pointing from the center of the planet to the tilt axis
$\hat{\mathbf{o}}$	Unit vector from the star to the observer
$\hat{\mathbf{s}}$	Unit vector describing a point on the exoplanet in the coordinate system of the star
$\hat{\mathbf{p}}$	Unit vector describing a point on the exoplanet rotating with the planet
θ	Polar angle/latitude
ϕ	Azimuth angle/longitude
β	Obliquity of the exoplanet
α	Angle between Vernal equinox of the exoplanet and the observer
$M(\theta, \pi)$	Albedo map of an exoplanet
$\mathbf{M}$	Map vector in the Y_l^m basis
$f(t)$	The light curve
$\mathbf{f}$	Vector of Fourier coefficients

Abstract

This thesis develops a method to map the surface of an exoplanet. The problem of exoplanet mapping sounds easy to solve. Take a few photographs of an exoplanet and sew them together to create a map of the surface. The telescope required to do this is far beyond our technological capabilities. However, our current telescopes could allow us to measure the light reflected from the star on the surface of the star as a point source. This thesis constructs the surface map of an exoplanet using only a point source of reflected light as information. This method of planet mapping is called spin-orbit tomography, introduced by Cowan and Agol [2008] and more in depth by Fujii and Kawahara [2012]. Spin-Orbit tomography is a method to construct a surface map from the reflected light curve, the total intensity of the light from the star, reflected on the surface of the planet, directed towards an observer.

The mentioned papers split the surface map into finite sized pixels. This report constructs a surface map from spherical harmonics and describes the reflected light from the exoplanet as its Fourier coefficients, this new variant of Spin-orbit tomography was first introduced by Van Oosterom [2019]. Van Oosterom [2019] assumed Lambertian reflection of light. This paper assumes Fresnel reflection of light. Fresnel reflection means that only water reflects light. Van Oosterom [2019] and this report develop a linear transformation from the surface map to the light curve, as both reports also assume different forms of reflection, the reports could easily be combined.
For this method of spin-orbit tomography we use that the signal is quasi periodic due to diurnal and annual motion. The advantages of this method are that it uses a standard basis for the map and the time signal, it mostly allows for analytical expressions for the relation between the time signal and the surface map and the Fourier coefficients allow noise to be filtered out. The disadvantages are that it assumes the axial tilt of an exoplanet to be known and small. Because only water reflects light, the surface map is a map of zeros and ones, this gives rise to the Gibbs phenomenon when approximating a map wit the spherical harmonics.

We derive a transfer matrix which gives the reflective light-curve under the assumptions that the orbit of the exoplanet is circular, the absence of clouds, the absence of moons, general time-invariance of the surface map, light is not absorbed by the atmosphere and the axial tilt is known and small. The transfer matrix found was independent of the surface map, making it widely applicable. The transfer matrix only depends on the orientation of the orbit of the exoplanet and the axial tilt of the exoplanet. In this report we assumed that either the orbit of the planet is in the plane of the observer, called edge-on observation. Or the orbit of the planet is perpendicular to the observer. The transfer matrix gives the light-curve if the surface map is known. However, we are interested in the inverse problem. The transfer matrix is not invertible. The Moore-Penrose pseudoinverse was used instead of the normal inverse. Part of the surface map is lost due to the nature of how light reflects on water. Only a band on the exoplanet could reflect light towards the observer, the information outside of this band never reaches the observer so information outside this band is lost. Further study might find a more general transfer matrix without the need to specify face-on or edge-on observation. Or further study could aim to find the axial tilt of the exoplanet.

Contents

Introduction

Exoplanets

The idea of a planet is ancient, with the Babylonians being the first civilization known to have a functional theory of the planets. With the first mention of planetary text probably dating back to as early as the second millennium BC. Only after the invention of the telescope, all eight planets in our Solar system were discovered, with Neptune discovered in 1846.
However, the notion that a planet might not be unique to our solar system can be dated back to the sixteenth century. Giordano Bruno, an Italian philosopher, suggested that the distant stars might be similar to the sun, implying the whole solar system to be comparable. With that the idea of exoplanets was born. After the idea was mentioned again by Isaac Newton in his Principia, support for the idea of exoplanets began to grow.
Although the idea of an exoplanet dates back to the sixteenth century, due to the limitation in instrumental capabilities, it took until 1989 (NASA [2021]) for the first discovery. Since then, the detection methods for exoplanets have been greatly improved and there are currently 4514 confirmed discoveries with 7721 candidates awaiting confirmation (NASA [2021]).

The discovery of exoplanets

There are five common methods used to discover exoplanets (NASA [2021])

1. Radial Velocity, small movements of the star due to the gravitational pull of the exoplanet cause a doppler shift in the light from the star.
2. Transit Method, an exoplanet moving in front of the star blocks a small part of the light from the star.
3. Direct Imaging, by removing the glare of the star, the reflected light from the star on the exoplanet can be measured.
4. Gravitational Microlensing, the light from the star is bent due to the gravity of the exoplanet.
5. Astrometry, the star wobbles due to the orbit of the exoplanet and its gravitational pull. This small wobble can be measured.

Of these five methods to discover exoplanets, four of them are indirect measurements, meaning a measurement on the light of the star is done to prove the presence of an exoplanet. Only the direct imaging method measures the planet itself. The radial velocity and transit method are used the most to discover exoplanets. The aim of this report is to map the surface of an exoplanet by measuring the light reflected on the surface of the exoplanet. For this, we take a closer look at the direct imaging method.

Direct Imaging

The light from a star is orders of magnitude brighter than the light reflected off the surface of the exoplanet. So actually measuring a planet itself is extremely difficult. New techniques and rapidly-advancing technology are making this happen. There are instruments designed, called shine blockers, to directly image exoplanets. Here, the light of the star is blocked. With the glare from the star reduced, you can get a better look at objects around the star that might be exoplanets. This report goes into the information inside the light signal reflected on the surface of the exoplanet. Determining the surface of exoplanets might begin to answer fundamental questions about the universe and our place in it. One of

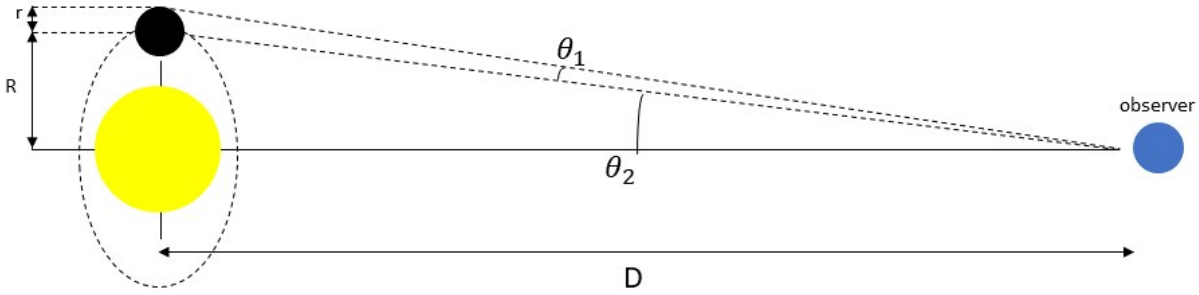

Figure 1: The required angular resolution required for observation of exoplanets. An exoplanet with radius r is orbiting a star at distance R. A telescope which could measure an angle of θ_1 could take a photograph of the surface of an exoplanet. A telescope which could measure an angle of θ_2 could measure the reflected light of an exoplanet as a point source.

the ultimate goals in the study of exoplanets is to answer the question of extraterrestrial life and if there are habitable exoplanets. For this reason, we are mainly interested in planets inside the habitable zone, or "Goldilocks zone", this zone is the area around a star where liquid water could exist on the surface of a planet. Life on Earth started in water, and water is a necessary ingredient for life as we know it. The habitable zone is also a main reason why this report looks at the reflection of water on the surface of an exoplanet.
The problem with the mapping of exoplanets is of the obvious kind, the limits of human technology. If a telescope could enhance a picture of an exoplanet enough to get a spatial resolution, taking a few photographs over time could give us a reasonable way to sew together a map of the exoplanet. This could be achieved with a telescope with an angular resolution of at least $\theta_1 \approx r/D$ (see figure 1), with r being the radius of the exoplanet and D the distance between the observer and the exoplanet. Then the size of the telescope needed can be found from the Rayleigh criterion:

$$d_1 = 1.22\frac{\lambda}{\theta_1} \approx 1.5 \text{ km} \tag{1}$$

Where d_1 is the required diameter of the telescope. λ is the wavelength of the measured light. So a telescope with $d = 1.5$ km is required to measure an exoplanet with the diameter of Earth (12.742 km) orbiting around the closest star (Proxima Centauri, 4.2441 ly, Wikipedia contributors [2021]), where we assume to measure blue light ($\lambda = 400$ nm). Mapping an exoplanet using this method, even considering the closest solar system, is beyond our technological capabilities. This reports studies objects so distant that they remain unresolved point sources.

A method to obtain information from an unresolved point source

Consider an exoplanet in orbit around a star, one half of the planet is illuminated by the star. Another half of the exoplanet is visible to the observer. As the exoplanet orbits around its star, the part that is illuminated and the part that is visible to the observer both change. As an exoplanet spins around its axis, the surface that is visible to the observer and illuminated by the star also changes. Depending on the type of surface, light is reflected differently. Because of this, the light curve is a function of the surface map. This report attempts to solve the inverse problem, from the light curve we try to find the surface map. Numerous reports go into the problem of exoplanet mapping Cowan and Agol [2008], Fujii et al. [2010], Fujii et al. [2011], Fujii and Kawahara [2012]. They also introduced the name that this technique goes by: Spin-Orbit Tomography (or SOT). The mentioned reports split up the surface map of the exoplanet into discrete parts. Over time, each part contributes to the light signal in its own specific manner.
In this report, a new variation of SOT is explored, this report builds on the results from Van Oosterom [2019]. The techniques in this report to reconstruct the surface map of an exoplanet require the angle with which we look at the star system, called the inclination I, and the axial tilt, described with the azimuth and polar angle α and β. The inclination can be obtained by observing the solar system and assuming the orbit of the exoplanet is circular. This could be achieved with a telescope with an angular resolution of at least $\theta_2 \approx R/D$ (see figure 1), with R being the radius of the orbit of the exoplanet.

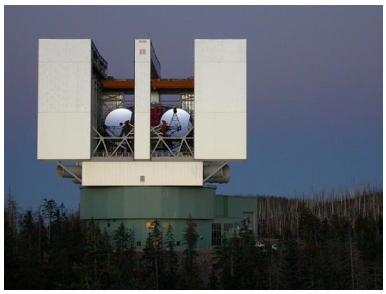


Figure 2: The Large Binocular Telescope on the left with a photograph it took of Messier 57 - The Ring Nebula on the right LBTO [2020].

Again, the size of the telescope needed can be found from the Rayleigh criterion:

$$d_2 = 1.22\frac{\lambda}{\theta_2} \approx 0.13 \text{ m} \tag{2}$$

Where d_2 is the required diameter of the telescope. λ is the wavelength of the measured light. So a telescope with $d = 0.13$ m is required to measure the inclination of the solar system. Where we assumed the radius of orbit to be equal to the distance between the Earth and the Sun (0.000016 ly) and assuming we measure on the closest star (Proxima Centauri, 4.2441 ly). The requirement of telescope size translate linearly over distance, so with the Large Binocular Telescope (figure 2) having an effective aperture of 11.9 m, we could perform this measurements on solar systems almost hundred times further than Proxima Centauri.

In this report, instead of splitting the map up into finite sized pixels, the map is decomposed into spherical harmonics and the light signal into its frequency components (Fourier coefficients). This report also only considers Fresnel reflection, meaning water reflects light, land mass does not. Van Oosterom [2019] assumed the opposite, only Lambertian reflection (land mass reflects light) and no Fresnel reflection (water does not reflect light).
The decomposition into spherical harmonics and Fourier coefficients has a number of advantages:

1. The spherical harmonics and Fourier coefficients form a complete basis for the map and signal, because the light signal depends on the diurnal and annual rotation of the exoplanet we only have a discrete number of frequencies in the light signal, therefore the Fourier coefficients form a complete base.

2. Because the spherical harmonics and the Fourier coefficients are discrete, the transformation matrix between the spherical harmonics and Fourier coefficients is linear, therefore results obtained outside of this report can easily be combined with the results from this report.

3. The transformation from the surface map to the signal can mostly be expressed in analytical terms to give better insight.

4. By splitting the time signal into its frequency components noise can be filtered out.

The disadvantages of this method are:

1. In the analytic calculation we use the small angle approximation for the axial tilt, so the method developed in this report is only applicable for small values of axial tilt.

2. The surface map is a discontinuous function. As we construct the surface map from a finite number of spherical harmonics, the Gibbs phenomenon occurs.

This report has been divided into four chapters, the first chapter goes into the properties of the reflective light curve. The second chapter introduces the spherical harmonics and how we use them to reconstruct a surface map. The third chapter introduces the transfer matrix, a matrix that defines the relation between a surface map and the light signal. The final chapter elaborates on the inverse of this problem and constructs a surface map from a light signal.
To obtain these results, a couple of assumptions are made throughout this report:

1. Circular orbit of the planet around the star.
2. Absence of clouds in the atmosphere.
3. Absence of moons orbiting the planet.
4. General Time-invariance of the surface map, for example: there are no ice caps that grow or shrink during different seasons and snow also does not affect the reflectivity off the surface of the planet.
5. Light is not affected by the atmosphere.
6. The axial tilt, defined by the angles α and β is known and β is assumed to be small.

This bachelor thesis has been supervised by Dr. Paul Visser and Dr. Aurèle Adam. For a report decomposing the surface map into spherical harmonics and the light signal into its frequency components using Lambertian reflection, see Van Oosterom [2019].

Chapter 1

The reflective light curve

In this chapter we see how we can describe a light-curve. The light-curve is a signal over time dependent on the reflective properties of an exoplanet, more precisely the light reflected on the surface of an exoplanet directed towards the observer. To describe the light-curve we introduce the parameters that describe the planet we intend to observe. Next, this chapter goes into how the surface and the orientation of the planet influence the light-curve. This is divided into two main parts, the location of the reflection point and the intensity of the reflected light.

1.1 Parameters

In this report we consider a solar system with a star located at the origin. The solar system has one planet, moving in circular orbit with radius R around the star. We describe the circular motion of the exoplanet around the star with the angular frequency ω, and the location of the exoplanet with the vector $\mathbf{r}$, the angle corresponding to this motion is γ with $\gamma = \omega t$. The planet also moves around its own axis $\hat{\mathbf{n}}$, with angular frequency Ω, the current angle of axial tilt will be described using Γ, so $\Gamma = \Omega t$.

	Angular frequency	Angle
Spin	Ω	$\Gamma = \Omega t$
Orbit	ω	$\gamma = \omega t$

We set the basis vectors $\hat{\mathbf{x}}$, $\hat{\mathbf{y}}$ and $\hat{\mathbf{z}}$ such that the x-y plane is the orbital plane. The observer of the system is on Earth with time-independent position $\mathbf{o}$, in this report we assume the distance between the observer and the exoplanet is orders of magnitude larger than the radius of the solar system, as we consider exoplanets in different solar systems than Earth, this not a real restriction. We fix $\hat{\mathbf{x}}$ to be parallel to the projection of $\hat{\mathbf{o}}$ on the x-y plane. The vectors introduced are easiest to write in spherical coordinates and given as follows:

$$\mathbf{r} = R\begin{pmatrix}\cos(\gamma)\\ \sin(\gamma)\\ 0\end{pmatrix}, \quad \hat{\mathbf{n}} = \begin{pmatrix}\cos(\alpha)\sin(\beta)\\ \sin(\alpha)\sin(\beta)\\ \cos(\beta)\end{pmatrix}, \quad \mathbf{o} = R_o\begin{pmatrix}\cos(I)\\ 0\\ \sin(I)\end{pmatrix} \tag{1.1}$$

The position $\mathbf{r}$ of the exoplanet is a function of time. The axial tilt $\hat{\mathbf{n}}$ of the exoplanet is described by the parameters α and β, which are time-independent. The angle I is the inclination of the observer. Have a look at figure 1.1 and figure 1.2 for clarity.

Remark. *In this report, there are two special cases of the inclination we are interested in, we call these the face-on and the edge-on observations. The face-on observation is for $I = \pi/2$. In this case the observer is perpendicular to the orbital plane of the exoplanet. $I = 0$ for edge-on observations. In this case the observer is in the orbital plane of the exoplanet.*

1.2 Measuring the light signal from an exoplanet

The first thought when constructing a surface map of an exoplanet would be to take a few photographs of the exoplanet the same way we could create a surface map of a moon by taking a few photographs over

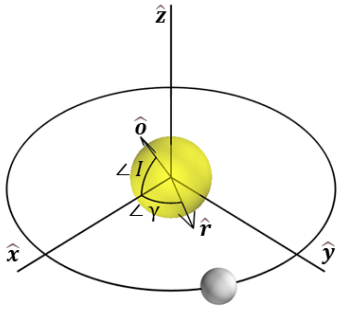

Figure 1.1: The planet is moving in a circular orbit in the xy-plane, making an angle $\gamma = \omega t$ with the x-axis. $\hat{\mathbf{r}}$ is a basic vector pointing at the exoplanet, $\hat{\mathbf{o}}$ is the basic vector pointing at the observer, making an angle I with the x-axis in the xz-plane.

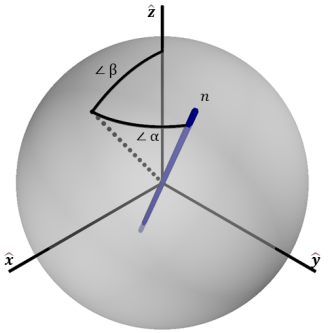

Figure 1.2: The exoplanet has a tilt axis n with rotational frequency Ω around this axis. The parameters α and β define the tilt axis as shown in the image.

time and sewing them together. However, in the introduction we calculated the size of a telescope needed to photograph the surface of an exoplanet. A telescope with a diameter of roughly 1.5 km would be needed to take a photograph of the surface of an exoplanet in the closest solar system to the sun, whereas a telescope with a diameter of roughly 0.13 m is needed to measure a point source of light reflected from the surface of an exoplanet in the same solar system. This report works with the assumption that we can measure a point source of reflected light from the exoplanet. This report considers Fresnel reflection.

1.3 Fresnel reflection

The Fresnel equations describe the reflection and transmission of light when incident on an interface between different optical media. In this report we make the assumption that the surface of a planet can either be land or water. As land is not an optical medium, in this report, we assume the land does not reflect light. In other words, by looking at the Fresnel reflection we assume only water reflects light. The intensity of light reflecting on water is dependent on the angle of incidence θ_i. The Fresnel equations give the reflection coefficients for s-polarized light and p-polarized light as follows.

$$R_s = \left(\frac{n_2 \cos\theta_i - n_1 \cos\theta_t}{n_2 \cos\theta_i + n_1 \cos\theta_t} \right)^2 \tag{1.2}$$

$$R_s = \left(\frac{n_2 \cos\theta_t - n_1 \cos\theta_i}{n_2 \cos\theta_t + n_1 \cos\theta_i} \right)^2 \tag{1.3}$$

Where n_1 is the refraction index of the media through which the incoming wave travels, which is air, with $n = 1$. n_2 is the refraction index of the media the transversed wave travels through, which is water, with $n = 4/3$. θ_i is the angle of incidence, θ_t is the angle of transmission. These can be linked using Snell's law

$$n_1 \sin(\theta_i) = n_2 \sin(\theta_t) \tag{1.4}$$

The Fresnel equations assume the interface between media is flat and that the media are homogeneous and isotropic. The incident light is assumed to be a plane wave. We assume these assumptions hold on an exoplanet. The light wave coming in from a star is unpolarized, that means that the reflectivity is the average of that for s and p polarization

$$f = R_e = \frac{R_s + R_p}{2} = \frac{49(9 - 11\cos^2(\theta_i) + 18\cos^4(\theta_i)}{(21 + 75\cos^2(\theta_i) + 25\cos(\theta_i)\sqrt{7 + 9\cos^2(\theta_i)})^2} \tag{1.5}$$

We find θ_i from Eq. 1.12

$$\cos(\theta_i) = \hat{\mathbf{s}} \bullet \hat{\mathbf{o}} = \frac{\sqrt{2}}{2}\sqrt{1 - \cos(\omega t)\cos(I)} \tag{1.6}$$

For light reflecting on water, the law of reflection holds:

$$\theta_i = \theta_r \tag{1.7}$$

The angle of the incoming light θ_i is equal to the angle of the reflected light θ_r.

The intensity of reflected light considering face-on observation

For the intensity of the light signal we are also interested in the two cases for the inclination. We start with a face-on observation. The orbit of the exoplanet is perpendicular to the observer, so $I = \pi/2$. Then the angle of the incoming light becomes

$$\cos(\theta_i) = \frac{\sqrt{2}}{2} \tag{1.8}$$

Filling this into Eq. 1.5 gives a constant intensity of the reflected light, $f = 0.0279$. This means the light signal becomes an identity function, returning 0 for reflection on land, and having an intensity of 0.0279 for reflection on water.

The intensity of reflected light considering edge-on observation

Secondly, we look at an edge-on observation, $I = 0$. The observer is in the plane of orbit of the exoplanet. The angle of the incoming light is now

$$\cos(\theta_i) = \frac{\sqrt{2}}{2}\sqrt{1 - \cos(\omega t)} = |\sin(\omega t/2)| \tag{1.9}$$

We can fill this result into Eq. 1.5 to find the intensity of the reflected light for a water world observed edge-on. This gives the following equation for the intensity

$$\frac{98(16 - 7\cos(\omega t) + 9\cos^2(\omega t)}{(117 - 75\cos(\omega t) + 25\sqrt{1 - \cos(\omega t)}\sqrt{23 - 9\cos(\omega t)})^2} \tag{1.10}$$

We plot this equation in figure 1.3. The peak we see is around the eclipse. Keep in mind that this plot is for reflection on water On land, the reflection would be zero.

1.4 The location of the glint

In the previous section we saw that the light curve depends on the type of surface the light hits and the angle of incidence. From 1.7 we see that the angle of incidence is equal to the angle of reflection, implying that there is a specific location on the exoplanet for which a light wave hitting water is reflected towards the observer. We call this specific location 'the location of the glint'. We would like to relate the location of the glint to the surface. If we have the location of the glint over time on the exoplanet, the light-curve could be calculated if the surface map of an exoplanet is known. We denote the location of the glint with two vectors $\hat{\mathbf{s}}$, and $\hat{\mathbf{p}}$. We use $\hat{\mathbf{s}}$ to describe the location of the glint in the coordinate system of the solar system and we use $\hat{\mathbf{p}}$ in the coordinate system rotating with the planet, which we can use to link a surface map to the light-curve. From eq. 1.7 we can express the location of the glint in terms of the parameters we introduced before.

$$\hat{\mathbf{s}} = \frac{\hat{\mathbf{o}} - \hat{\mathbf{r}}}{|\hat{\mathbf{o}} - \hat{\mathbf{r}}|} \tag{1.11}$$

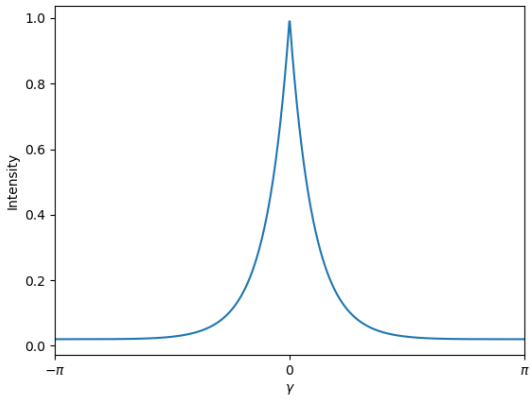

Figure 1.3: The time signal for the intensity of the reflection that is directed towards Earth for a water world in case of an edge-on observation. The peak in the graph is for $\gamma = 0$, this happens when the planet is in front of the star. This means that the star is eclipsed for a short time.

From Eq. 1.1 we get

$$\hat{\mathbf{s}} = \frac{1}{\sqrt{2 - 2\cos(I)\cos(\omega t)}} \begin{pmatrix} \cos(I) - \cos(\omega t) \\ -\sin(\omega t) \\ \sin(I) \end{pmatrix} \tag{1.12}$$

We see that for a certain value of I and t, the glint location $\hat{\mathbf{s}}$ is undefined. Which is the case for $I = 0$ and $t = 2k\pi/\omega$. This is known as an eclipse, the exoplanet is exactly in between the star and the observer. Later in this report we go deeper into the glint location for edge-on observations. There we also tackle the problem of an eclipse.

The glint location considering face-on observation

As remarked before, we are interested in two special cases for the inclination. Here we go into the location of the glint specifically for a face-on observation, so $I = \pi/2$. This gives

$$\hat{\mathbf{s}} = \frac{1}{\sqrt{2}} \begin{pmatrix} -\cos(\omega t) \\ -\sin(\omega t) \\ 1 \end{pmatrix} \tag{1.13}$$

The location of the glint can be shown with figure 1.4. From Eq. 1.13 we can calculate that the polar angle is given as $\theta = \pi/4$ and the azimuth angle is $\phi = \pi + \omega t$.

The exoplanet rotates around the star and spins around its own axis. The surface the glint hits changes the light curve we measure depending on whether the glint moves over water or land. So we want to relate the vector $\hat{\mathbf{s}}$ to a certain position on the surface of the exoplanet.
Transforming from the coordinate system of the star to the frame of reference of the exoplanet means we have to account for the rotation of the planet around its own axis. The tilt axis of a planet is given as the vector $\hat{\mathbf{n}}$ in Eq. 1.1 with the parameters of α and β. In the case of a face-on observation we can change our coordinate system in a smart way such that the axial tilt can be described only using the variable β. For this we recall that $\hat{\mathbf{x}}$ is chosen such that it is parallel to the projection of $\hat{\mathbf{o}}$ on the x-y plane. But $\hat{\mathbf{o}} = \hat{\mathbf{z}}$, thus we are free to choose $\hat{\mathbf{x}}$ how we like. We can fix $\hat{\mathbf{x}}$ to be parallel to the projection of $\hat{\mathbf{n}}$ on the x-y plane, this makes $\alpha = 0$. Realise that the position of the exoplanet is the only time dependent thing in the coordinate system of the exoplanet, so fixing $\hat{\mathbf{x}}$ has the same effect as changing the choice for $t = 0$, which can be done because the system is time-invariant. To relate the location of the glint to a position on the exoplanet we have the following

$$\hat{\mathbf{s}}(\mathbf{t}) = R_z(\Omega t) R_y(\beta) \hat{\mathbf{p}}(\mathbf{t}) = R_z(\Gamma) R_y(\beta) \hat{\mathbf{p}}(\mathbf{t}) \tag{1.14}$$

Where we rotate along the z axis to account for the daily rotation of the planet around its tilt axis and we rotate along the y axis to account for the actual tilt axis. The functions R_z and R_y denote the rotation matrices.

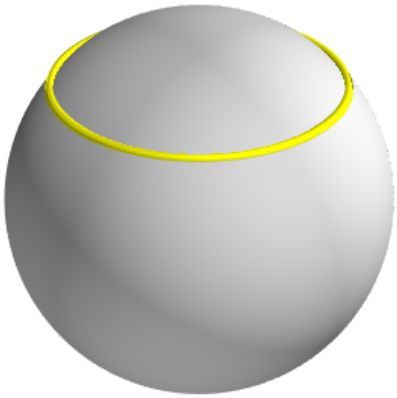

Figure 1.4: The location of the glint for a face-on observation. The glint moves on a latitude of $\pi/4$, with the azimuth angle equal to $\pi + \omega t$, so making a single rotation per year.

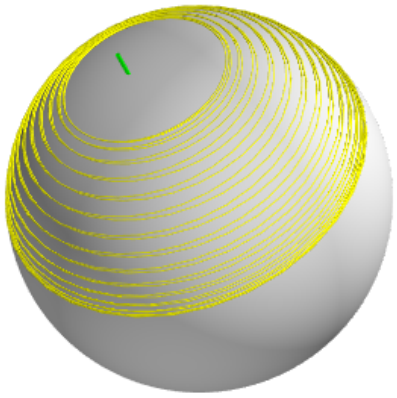

Figure 1.5: The location of the glint on a planet. Tilt $\beta = \pi/8$, $\Omega = 30\omega$. The yellow line shows the location of the glint over time, green shows the spin axis of the exoplanet. The band is centered around a latitude of $\pi/4$, which is the case for all face-on observations, the tilt β influences the width of the band. We roughly see that the azimuth angle is influenced by the diurnal rotation and the polar angle is influenced by the annual rotation.

$$R_z(\theta) = \begin{pmatrix} \cos(\theta) & -\sin(\theta) & 0 \\ \sin(\theta) & \cos(\theta) & 0 \\ 0 & 0 & 1 \end{pmatrix} \qquad R_y(\theta) = \begin{pmatrix} \cos(\theta) & 0 & \sin(\theta) \\ 0 & 1 & 0 \\ -\sin(\theta) & 0 & \cos(\theta) \end{pmatrix} \tag{1.15}$$

So we get the following equation for $\hat{\mathbf{p}}$, where the inverse of a rotation matrix is the same as rotating around the negative angle:

$$\hat{\mathbf{p}}(\mathbf{t}) = R_z(-\Omega t) R_y(-\beta) \hat{\mathbf{s}}(\mathbf{t}) \tag{1.16}$$

We can work out this expression and we get the following

$$\hat{\mathbf{p}}(\mathbf{t}) = \frac{\sqrt{2}}{2} \begin{pmatrix} -\sin(\Omega t)\sin(\omega t) - \sin(\beta)\cos(\Omega t) - \cos(\Omega t)\cos(\beta)\cos(\omega t) \\ \sin(\Omega t)\sin(\beta) + \sin(\Omega t)\cos(\beta)\cos(\omega t) - \sin(\omega t)\cos(\Omega t) \\ -\sin(\beta)\cos(\omega t) + \cos(\beta) \end{pmatrix} \tag{1.17}$$

This equation gives the location of the glint in the reference frame of the planet. To better see how the location of the glint moves over time we take a look at figure 1.5. We see that the azimuth angle has a daily frequency, whereas the polar angle has a yearly frequency.

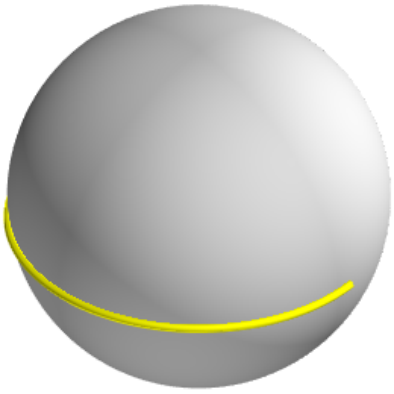

Figure 1.6: The location of the glint for an edge-on observation in the coordinate system of the observer, so the axial tilt is not taken into account. The glint moves on a latitude of $\pi/2$, along the equator. The azimuth angle only makes half a circle.

The location of the glint considering edge-on observation

Secondly, we evaluate the case of an edge-on observation, $I = 0$. This gives

$$\hat{\mathbf{s}} = \frac{1}{\sqrt{2 - 2\cos(\omega t)}} \begin{pmatrix} 1 - \cos(\omega t) \\ -\sin(\omega t) \\ 0 \end{pmatrix} \tag{1.18}$$

We can work out the square root in front of the vector. We use trigonometric identities to work Eq. 1.18 out to the following:

$$\hat{\mathbf{s}} = \begin{pmatrix} \sin(\omega t/2) \\ -\cos(\omega t/2) \\ 0 \end{pmatrix} \sigma(\sin(\omega t/2) \tag{1.19}$$

Where σ is the sign function. This equation is still undefined in the case of an eclipse, or

$$t = 2k\pi/\omega, \quad k \in \mathbb{Z}$$

To better understand the behaviour of the glint location. we evaluate what happens mathematically during an eclipse. This is done by working out these two limits:

$$\lim_{t\to 0^-} \hat{s}(t), \quad \lim_{t\to 0^+} \hat{s}(t) \tag{1.20}$$

$$\lim_{t\to 0} \hat{s}(t) = \lim_{t\to 0} \begin{pmatrix} \sin(\omega t/2) \\ -\cos(\omega t/2) \\ 0 \end{pmatrix} \sigma(\sin(\omega t/2)) \tag{1.21}$$

Only the y coordinate is undefined for $t = 0$.

$$\lim_{t\to 0^+} -\cos(\omega t/2)\sigma(\sin(\omega t/2)) = \lim_{t\to 0^+} -\cos(\omega t/2) = -1 \tag{1.22}$$

$$\lim_{t\to 0^-} -\cos(\omega t/2)\sigma(\sin(\omega t/2)) = \lim_{t\to 0^-} \cos(\omega t/2) = 1 \tag{1.23}$$

This means that the glint location makes a jump from one side of the planet to the other side. Which is not surprising. Compared to the observer, the planet makes a jump from one side of the star to the other side.
The location of the glint can be shown with figure 1.6. We see the glint forms a half circle on one side of the planet. During one annual rotation, the glint makes half a circle. Then, during an eclipse, the glint location jumps to the other side. As before, we relate the vector $\hat{\mathbf{s}}$ to a certain position on the surface of the exoplanet. Again, we take the tilt axis and the rotation around the spin axis into account. For face-on observations we could ignore the parameter α. This is not possible for edge-on observations

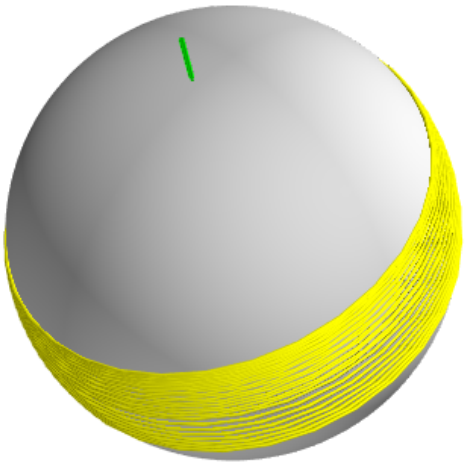

Figure 1.7: The location of the glint on a planet for an edge-on observation. Tilt $\alpha = \beta = \pi/8$, $\Omega = 30\omega$. The yellow line shows the location of the glint over time, green shows the spin axis on the exoplanet. The band is centered around the equator, which would be the case for any edge-on observation, α and β influence the band itself. We roughly see that the azimuth angle is influenced by the diurnal rotation whereas the polar angle is mainly influenced by the annual rotation.

because $\hat{\mathbf{x}}$ is defined from the observer. To relate the location of the glint to a position of the exoplanet we have the following relation

$$\hat{\mathbf{s}}(\mathbf{t}) = R_z(\alpha)R_y(\beta)R_z(\Omega t - \alpha)\hat{\mathbf{p}}(\mathbf{t}) \tag{1.24}$$

We rotate around the z-axis by $\Omega t - \alpha$ instead of Ωt, we can do this because Ωt is for the daily rotation and we can arbitrarily choose $t = 0$ for the daily rotation. This leads to a simpler expression, which we see in chapter 3. This means we get the following equation for $\hat{\mathbf{p}}$. Keep in mind that R_y and R_z are rotation matrices for which the inverse is the same as rotating around the negative angle.

$$\hat{\mathbf{p}}(\mathbf{t}) = R_z(-(\Omega t - \alpha))R_y(-\beta)R_z(-\alpha)\hat{\mathbf{s}}(\mathbf{t}) \tag{1.25}$$

This results in a long equation which I will not write out in this report, but which an be calculated analytically. As before, we take a look at figure 1.7. We see that the band in which the glint moves is centered around the equator.

Chapter 2

Model surface maps of exoplanets

The goal of this report is to recover a surface map. For this chapter 1 derived what kind of information the light-curve contains, the next chapter calculates a linear transformation giving the light curve as a function of a surface map. This chapter goes into the surface maps themselves. This chapter elaborates how and why the spherical harmonics are used in this report. Furthermore, this chapter describes two algorithms to generate a surface map and calculates the spherical harmonics for a few examples.

2.1 Spherical Harmonics

Spherical harmonics are functions defined on the surface of a sphere. The definition of the spherical harmonics used in this report is

$$M(\theta,\phi) = \sum_{l=0}^{\infty} \sum_{m=-l}^{l} M_l^m Y_l^m(\theta,\phi) \tag{2.1}$$

$$M_l^m = \frac{1}{4\pi} \int_0^{\pi} \int_0^{2\pi} M(\theta,\phi) Y_l^m(\theta,\phi) \sin(\theta) d\phi d\theta \tag{2.2}$$

The spherical harmonics are special functions defined on the surface of a sphere. In this report we use the following definition of the spherical harmonics

$$Y_l^m(\theta,\phi) = \sqrt{\frac{(2l+1)}{4\pi}\frac{(l-m)!}{(l+m)!}} P_l^m(\cos\theta) e^{im\phi} \tag{2.3}$$

Where $l \in \mathbb{N}_0$, $m \in \mathbb{Z} : -l \leq m \geq l$. θ is the polar angle and ϕ is the azimuth angle, P_l^m are the Associated Legendre polynomials, which have the closed form expression

$$P_l^m(x) = (-1)^m 2^l (1-x^2)^{m/2} \sum_{k=m}^{l} \frac{k!}{(k-m)!} x^{k-m} \binom{l}{k} \binom{\frac{l+k-1}{2}}{l} \tag{2.4}$$

The spherical harmonics are used for multiple reasons. They form an orthonormal basis, meaning any physical surface map can be written as the sum of spherical harmonics. The spherical harmonics also allows for analytical evaluations for the transfer matrix used for retrieval. Chapter 3 further goes into this matrix. The results obtained form the use of spherical harmonics make sure the results are more convenient to combine with the results of Lambertian retrieval, see Van Oosterom [2019].

With Eq. 2.1 we can calculate a surface map from the coefficients M_l^m. We introduce the map vector $\mathbf{M}$. Defined as

$$\mathbf{M} = \begin{pmatrix} M_0^0 \\ M_1^{-1} \\ M_1^0 \\ M_1^1 \\ \vdots \end{pmatrix}, \mathbf{M} \in \mathbb{C}^{\infty} \tag{2.5}$$

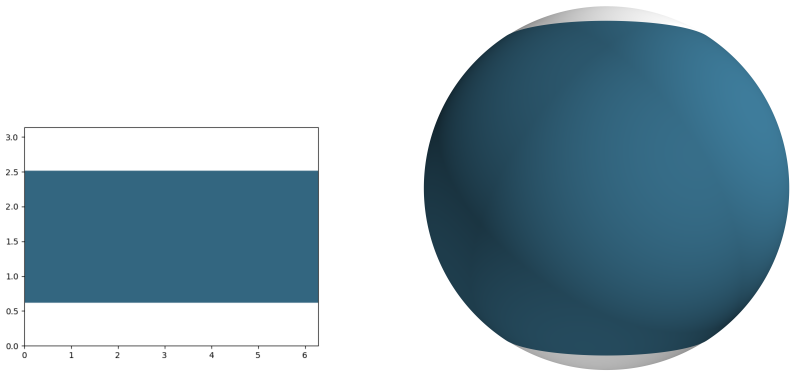

Figure 2.1: A planet map with ice caps at the north and south pole. The rest of the planet is covered with water. So the planet has water for $\{(\theta,\phi):\theta \in [\theta_c, \pi - \theta_c]\}$. For this plot $\theta_c = \pi/5$ is chosen. The left plot is a (θ,ϕ) plot of the map and the right plot is a 3d render.

A finite number of spherical harmonic coefficients will always result in a continuous surface function. As we are looking at the Fresnel reflection, with water reflecting light and land not reflecting light, the actual surface map is discrete. We limit ourselves to a maximum size of the map vector $\mathbf{M}$ with a set l_{max}, so then

$$\mathbf{M} = \begin{pmatrix} M_0^0 \\ M_1^{-1} \\ M_1^0 \\ M_1^1 \\ \vdots \\ M_{l_{max}}^{l_{max}} \end{pmatrix}, \mathbf{M} \in \mathbb{C}^{(l_{max}+1)^2} \tag{2.6}$$

The effect of l_{max} is shown in chapter 2.2.3.

2.2 Examples of maps

From Eq. 2.2 the coefficients of the spherical harmonics can be calculated if a surface map is known. The spherical harmonics are calculated for two simple maps, a world of water with two ice caps and a map with two continents of equal size. These maps are chosen because of their symmetry. In this report we look at the reflection of light on water, land does not reflect light. Therefore a function describing the surface of a planet is as simple as

$$M(\theta,\phi) = \begin{cases} 0 & (\theta,\phi) \text{ on land} \\ 1 & (\theta,\phi) \text{ on water} \end{cases} \tag{2.7}$$

2.2.1 The spherical harmonics for a planet with two ice caps

We first take a look at a planet with two ice caps, one at the north pole and one at the south pole. We assume that both ice caps have exactly the same size. This is a reasonable assumption because the amount of energy from the sun both poles get should roughly be the same. This map is interesting because it is symmetric, so the spherical harmonics should be relatively simple. This gives the following function for the map

$$M(\theta,\phi) = \begin{cases} 0 & \theta < \theta_c \vee \theta > \pi - \theta_c \\ 1 & \theta_c \leq \theta \leq \pi - \theta_c \end{cases} \tag{2.8}$$

Which looks as figure 2.1. To calculate the spherical harmonics, the calculations for a single ice cap can mostly be repeated. We get the following integral

$$M_l^0 = 2\pi\sqrt{4\pi(2l+1)} \int_{-\cos(\theta_c)}^{\cos(\theta_c)} P_l(u)du \tag{2.9}$$

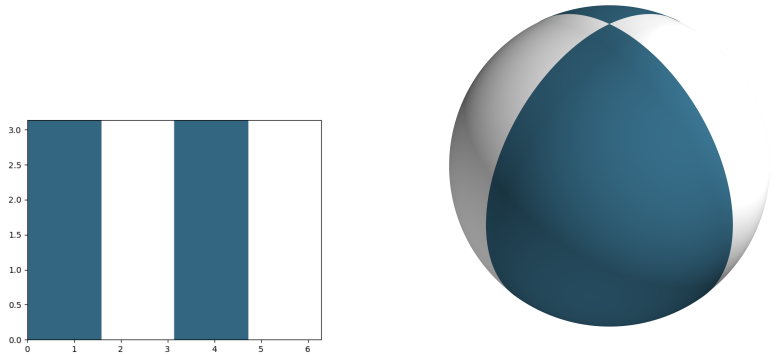

Figure 2.2: A planet map with two continents of equal size such that the map has mirror symmetry. The left image is a (θ,ϕ) plot, the right image is a 3D render.

Where we again get a nontrivial integral only for $m = 0$. Evaluating this integral results in

$$M_l^0 = 2\pi\sqrt{4\pi(2l+1)}\sum_{k=even}^{l}\binom{l}{k}\binom{\frac{l+k-1}{2}}{l}\frac{2\cos^{k+1}(\theta_c)}{k+1} \tag{2.10}$$

Because of the symmetric map, the expression for the spherical harmonics reduces to a simple expression.

2.2.2 The spherical harmonics for a planet with two continents

In the previous two paragraphs we looked at maps solely dependent on the polar angle. It was shown that the spherical harmonics, normally dependent on l, m, become solely dependent on l. In this paragraph, we look at a map solely dependent on the azimuth angle

$$M(\theta,\phi) = \begin{cases} 0 & \pi/2 < \phi < \pi \wedge 3\pi/2 < \phi < 2\pi \\ 1 & \phi \leq \pi/2 \wedge \pi \leq \phi \leq 3\pi/2 \end{cases} \tag{2.11}$$

Shown in figure 5. Filling in the function for the map into equation 2.2 gives

$$M_l^m = \frac{1}{4\pi}\sqrt{\frac{(2l+1)}{4\pi}\frac{(l-m)!}{(l+m)!}}\int_0^{\pi} P_l^m(\cos(\theta)\sin(\theta)d\theta\int_0^{2\pi} M(\phi)e^{im\phi}d\phi \tag{2.12}$$

2.2.3 Algorithms to compute surface maps

The maps mentioned previously give a nice insight into the spherical harmonics. But, to test the theory developed in this report, we use an algorithm to generate a random map. The aim is to be able to easily test the theory on multiple maps and to explore the limits of the retrieval method by making the maps nontrivial. Secondly, the aim is that an algorithm creates a surface map with continents. Continents imply big masses of land and water and might indicate that an exoplanet is similar to Earth.
This report describe two algorithms, the random circle algorithm, and the great circle algorithm. Both algorithms create a $m \times n$ bitmap, where an element of the bitmap corresponds to a (θ,ϕ) coordinate on the surface. We assume the planet is a perfect sphere so we can describe any coordinate on the planet with θ and ϕ.

The random circle algorithm

This section describes a way to generate a map with circles of random size. The algorithm works as follows

1. The parameters r, θ and ϕ are randomly generated n times.
2. The radii r are sorted.
3. The inside of the circle is alternately set to 0 or 1.

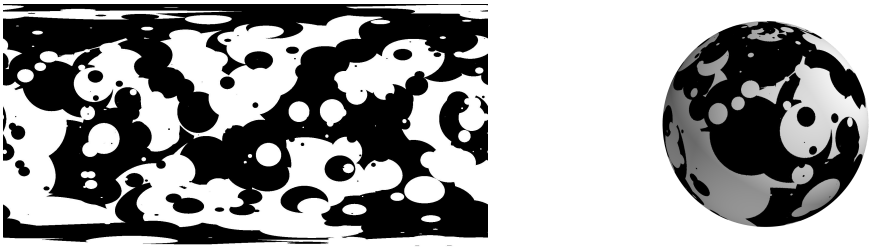

Figure 2.3: The random circle algorithm with $n = 1000$.

Figure 2.4: The Great-Circle algorithm with $n = 2000$. The left image shows a (θ,ϕ) plot of the map and the right plot is a 3D render.

This algorithm is tested to simulate lakes and islands on a planet. By generating a lot of circles, the border between land and water forms a nontrivial shape. The radii are sorted to draw the biggest circles first. If the radii are not sorted, one big circle overlaps a lot of small circles making the map much more trivial. Then we alternate setting a circle as 0 or 1 to allow a bigger n and to prevent a surface map to become either a water world or a land world. In figure 2.3 we see the algorithm executed to create a random map. The problem with this algorithm is that the circle shape still remains present, to better simulate our retrieval we would like a map which still has nontrivial borders between land and water but has bigger continent like shapes. Figure 2.3 uses the following equation to generate the radius of the circles

$$r_{circle} = 4/5 * r_{planet} * U(0,1)^{10} \tag{2.13}$$

We use this maximum radius because the circles generated with it look the best. We take the tenth power with the aim to create big continent like circles with smaller circles to simulate lakes/islands and make the border less trivial. We took $n = 1000$.

The Great-Circle Algorithm

The second algorithm we test is the great-circle algorithm. A great circle is a circle with the same radius as, in our case, the planet. So taking a great circle on a surface map means we split the map in half. The algorithm is as follows

1. Select a random great circle on the sphere.
2. Raise the altitude by a constant for the hemisphere on one side of the great circle, and lower the altitude by the same constant for the hemisphere on the other side.
3. Repeat this a large number of times (n).
4. In the end, if the altitude is negative, we set the bitmap to 0. If the altitude is not negative, we set the bitmap to 1.

The advantage this method offers is that the border between land and sea will seem a lot more natural. As this algorithm raises the altitude on one side of the hemisphere and lower the altitude on the other side, the map will be symmetric.

The spherical harmonics for the algorithms

We decompose the map from figure 2.4 and 2.3 where the decomposition is given by Eq. 2.1 and 2.2. These maps are way too complicated to do by hand so this will be done numerically using Python. Python

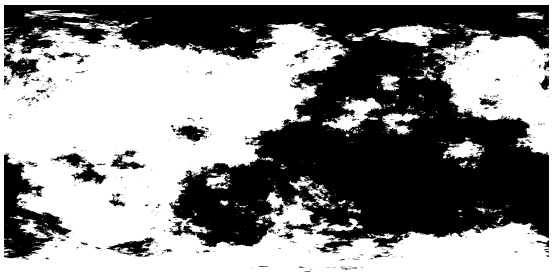

(a) Original map

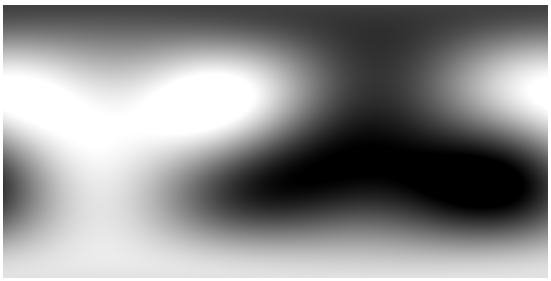

(b) $l_{max} = 4$

(c) $l_{max} = 10$

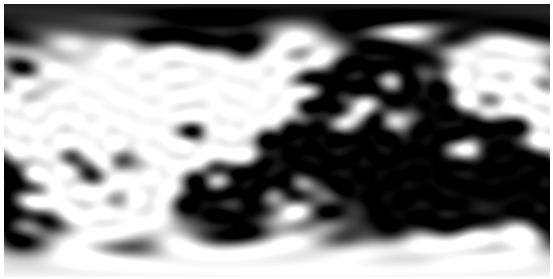

(d) $l_{max} = 25$

Figure 2.5: The effect of a different l_{max} for the spherical harmonics. The original map is generated using the Great-Circle algorithm (figure 2.5a. 2.5b, 2.5c and 2.5d are generated by calculating the integral from Eq. 2.2, then using the values found for M_l^m in Eq. 2.1. For the different maps, a different value of l_{max}, the resolution, is chosen.

cannot calculate an infinite number of coefficients so we limit ourselves to a certain value of l_{max}. Then

$$M(\theta, \phi) = \sum_{l=0}^{l_{max}} \sum_{m=-l}^{l} M_l^m Y_l^m(\theta, \phi) \tag{2.14}$$

The decomposition into spherical harmonics is shown in 2.5 and 2.6. In both these figures, the first image is the original map, with the other maps showing the map from the first spherical harmonic coefficients with a different value of l_{max}. We see that the value of l_{max} influences the sharpness of the surface map. However, for l_{max} large enough, the Gibbs phenomenon becomes apparent. Because we work with discrete maps and a spherical harmonics decomposition into finite coefficients will result in a continuous surface map, the Gibbs phenomenon occurs. To save on computation times, throughout this report we mostly work with $l_{max} = 4$, but for better retrieval, l_{max} could be increased.

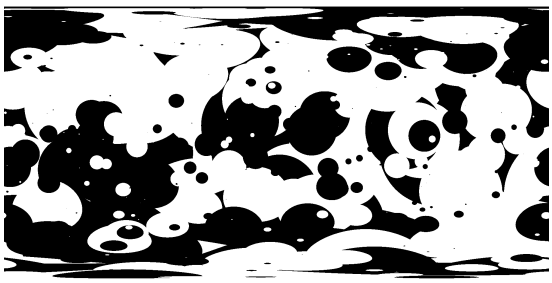

(a) Original map

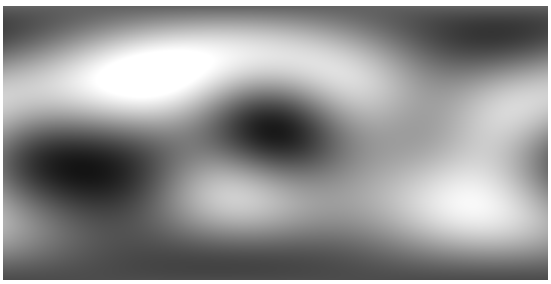

(b) $l_{max} = 4$

(c) $l_{max} = 10$

(d) $l_{max} = 25$

Figure 2.6: The effect of a different l_{max} for the spherical harmonics. The original map is generated using the Random Circle algorithm (figure 2.6a). 2.6b, 2.6c and 2.6d are generated by calculating the integral from Eq. 2.2, then using the values found for M_l^m in Eq. 2.1. For the different maps, a different value of l_{max}, the resolution, is chosen.

Chapter 3

From Surface map to light-curve

In this chapter we explore the relation between a surface map and the measured light signal. We find a matrix, which we call the transfer matrix. This matrix gives the light signal we would retrieve from a certain map. In the next chapter, we invert this function to be able to calculate a map from a measured signal.

3.1 Transfer Matrix

In chapter 2 we expressed a surface map in terms of a map vector $\mathbf{M}$. We do the same for the light-curve. The light-curve is split into its frequency components, or its Fourier coefficients. The signal is quasi periodic due to diurnal and annual motion of the exoplanet. Therefore, the Fourier coefficients span all possible light-curves an observer could receive. The Fourier coefficients of a light curve are defined as follows

$$f(\gamma, \Gamma) = \sum_{n=-\infty}^{\infty} \sum_{k=-\infty}^{\infty} f_k^n e^{i(k\gamma + n\Gamma)} \tag{3.1}$$

$$f_k^n = \frac{1}{(2\pi)^2} \int_0^{2\pi} \int_0^{2\pi} f(\gamma, \Gamma) e^{-i(k\gamma + n\Gamma)} d\gamma d\Gamma \tag{3.2}$$

Here we have replaced the signal function $f(t)$ with $f(\gamma, \Gamma)$, notice that $\gamma = \omega t$ and $\Gamma = \Omega t$. With ω and Ω constant, the function $f(\gamma, \Gamma)$ is still a function purely dependent on time.
The Fourier coefficient are calculated from the data collected by a telescope measuring the intensity of the reflected light from an exoplanet. In theory, a continuous intensity measurement would give the best results and the best calculations of the Fourier coefficients. However, it is more realistic that a telescope only measures over a period of time Δt.
Looking at Eq. 3.2, to be able to calculate the integral, the values of γ and Γ need to be varied independently. In the theoretical case, this would mean Ω/ω needs to be irrational. In the practical case, the higher the least common multiple of ω and Ω, the better the approximation of the integral. We continue this report assuming a continuous measurement with Ω/ω irrational, the reader should keep in mind that an actual measurement gives an approximation of the Fourier coefficients.
We express the Fourier coefficients as a vector of Fourier coefficients $\mathbf{f}$. We want to relate this vector $\mathbf{f}$ with the map vector $\mathbf{M}$. In this chapter we see that there is a linear transformation between the two, the transfer matrix A.
The transfer matrix is a matrix which relates the outputs of the system to its inputs. In this case, the system is the light reflection, the input is the ocean map of a planet, and the output is the light signal of the reflection that is directed towards Earth.

$$\mathbf{f} = A\mathbf{M} \tag{3.3}$$

with

$$\mathbf{f} = \begin{pmatrix} f_{-k_{max}}^{-n_{max}} \\ f_{-k_{max}}^{-n_{max}+1} \\ \vdots \\ f_{k_{max}}^{n_{max}} \end{pmatrix}, \mathbf{f} \in \mathbb{C}^{(2k_{max}+1)(2n_{max}+1)} \tag{3.4}$$

$$\mathbf{M} = \begin{pmatrix} M_0^0 \\ M_1^{-1} \\ M_1^0 \\ \vdots \\ M_{l_{max}}^{l_{max}} \end{pmatrix}, \mathbf{M} \in \mathbb{C}^{(l_{max}+1)^2} \tag{3.5}$$

The vector of Fourier coefficients $\mathbf{f}$ are the Fourier coefficients of the intensity of the reflected light, calculated with equation 3.2.
The map vector $\mathbf{M}$ is a construction of the original map, as done in chapter 2 with equation 2.2.
To calculate the transfer matrix, the Fourier coefficients for a fixed spherical harmonic are calculated, where we limit ourselves to $-2 \leq n, k \leq 2$ and $l_{max} = 3$. These values affect the size of the transfer matrix.
The signal function f can be written in terms of spherical harmonics:

$$f(\gamma, \Gamma) = \sum_{l=0}^{\infty} \sum_{m=-l}^{l} M_l^m I(\gamma) Y_l^m(\theta(\gamma, \Gamma), \phi(\gamma, \Gamma)) \tag{3.6}$$

In this equation, θ is the polar angle and ϕ is the azimuth angle. In chapter 1.4 we saw that the location of the glint was given as a function of time, thus as a function of γ and Γ. Meaning θ and ϕ are also functions of γ and Γ.
Because M_l^m is constant over varying γ, Γ we can take it out of the integral and form the calculation into a matrix multiplication, where an entry of the matrix A (so for fixed n, k, l, m) is given by

$$a_{i,j} = \int_0^{2\pi} \int_0^{2\pi} e^{-i(k\gamma + n\Gamma)} R_e(\gamma) Y_l^m(\theta(\gamma, \Gamma), \phi(\gamma, \Gamma)) d\gamma d\Gamma \tag{3.7}$$

The advantage this gives is that the matrix will be independent of the map. The matrix is purely depends on the way θ, ϕ depend on γ, Γ. This dependency in turn depends on α and β. Which is described in chapter 1.4. The θ, ϕ describe the location of the reflection point, θ being the polar angle and ϕ the azimuth angle. In chapter 1.4 we saw that this location depends on the inclination of the orbit of the planet I and the axial tilts α, β. This paper only studies the cases $I = 0$ and $I = \pi/2$.

3.2 Observing with face-on observation

First, the simpler case $I = \pi/2$. In chapter 1 we see that the intensity of the light is constant from Eq. 1.5. The value of α can also be ignored, because we can arbitrarily set an orientation of the planet as $t = 0$ as explained in chapter 1.4. The spherical harmonics are defined as

$$Y_l^m(\theta, \phi) = \sqrt{\frac{(2l+1)}{4\pi} \frac{(l-m)!}{(l+m)!}} P_l^m(\cos(\theta) e^{im\phi} \tag{3.8}$$

We intend to find an analytic expression for f_k^n by writing out an explicit expression for the associated Legendre polynomials and the exponential.
We start by taking $\beta = 0$. In chapter 1.4 the location of the glint is shown as

$$\hat{s}(t) = \frac{\sqrt{2}}{2} \begin{pmatrix} -\cos(\gamma - \Gamma) \\ \sin(\gamma - \Gamma) \\ 1 \end{pmatrix} \tag{3.9}$$

Where γ and Γ are substituted for ωt and Ωt respectively. This gives

$$\cos(\theta) = \frac{\sqrt{2}}{2}, \qquad \theta = \pi/4 \tag{3.10}$$

$$e^{i\phi} = -\cos(\Gamma - \gamma) + i \sin(\Gamma - \gamma), \qquad \phi = \gamma - \Gamma + \pi \tag{3.11}$$

Next, we look at a planet with axial tilt, where β is assumed to be small. As in chapter 1.4

$$\hat{p}(t) = R_z(-\Gamma)R_y(-\beta)\hat{s}(t) \tag{3.12}$$

Where we use the small β approximation for R_y

$$R_y(-\beta) = I + \begin{pmatrix} 0 & 0 & -\beta \\ 0 & 0 & 0 \\ \beta & 0 & 0 \end{pmatrix} \tag{3.13}$$

Working out the equation for $\hat{p}$ with this approximation for the rotation matrix gives

$$\hat{p}(t) = \frac{\sqrt{2}}{2}\begin{pmatrix} -\cos(\gamma - \Gamma) \\ -\sin(\gamma - \Gamma) \\ 1 \end{pmatrix} + \frac{\sqrt{2}}{2}\begin{pmatrix} -\beta\cos(\Gamma) \\ \beta\sin(\Gamma) \\ -\beta\cos(\gamma) \end{pmatrix} \tag{3.14}$$

As before, we want to find the azimuth angle ϕ and the polar angle θ. To find the azimuth angle we look at the complex plane, with the x component on the real axis and the y component on the imaginary axis. In the complex plane the following holds

$$e^{i\phi} \propto -e^{i(\gamma-\Gamma)} - \beta e^{-i\Gamma} \tag{3.15}$$

We can normalize the right hand side, which gives

$$e^{i\phi} = \frac{-e^{i(\gamma-\Gamma)} - \beta e^{-i\Gamma}}{\sqrt{1 + 2\beta\cos(\gamma) + \beta^2}} \tag{3.16}$$

As β is assumed to be small, the first order Taylor approximation is used.

$$e^{i\phi} = e^{i(\gamma-\Gamma)}[-1 + i\beta\sin(\gamma)] \tag{3.17}$$

The spherical harmonics use the m-th power, so

$$e^{im\phi} = e^{im(\gamma-\Gamma)}[-1 + i\beta\sin(\gamma)]^m \tag{3.18}$$

Which is simplified using the binomial approximation

$$e^{im\phi} = (-1)^m e^{im(\gamma-\Gamma)}[1 - im\beta\sin(\gamma)] \tag{3.19}$$

We are also interested in finding an explicit expression for the azimuth angle ϕ. We take the natural logarithm of eq. 3.17

$$i\phi = ln(e^{i(\gamma-\Gamma)}(-1 + i\beta\sin(\gamma)) \tag{3.20}$$

By taking the Taylor expansion we get the following

$$\phi = \gamma - \Gamma + \pi - \sin(\gamma)\beta \tag{3.21}$$

Now that we have found the azimuth angle, we move on to the polar angle, from 3.14

$$\cos(\theta) = \frac{\sqrt{2}}{2}(1 - \beta\cos(\gamma)) \tag{3.22}$$

Using the first order Taylor approximation after taking the arc cosine results in

$$\theta = \pi/4 + \beta\cos(\gamma) \tag{3.23}$$

We can check the formulas we find for θ, ϕ against the formulas we found without tilt. By filling in $\beta = 0$, we see that we get the same equations.
To evaluate the spherical harmonics we work out the associated Legendre polynomial $P_l^m(\cos(\theta)$. Applying the first order Taylor approximation results in

$$P_l^m(\cos(\theta)) = P_l^m(\sqrt{2}/2) + \frac{\sqrt{2}}{2}\frac{dP_l^m(c)}{dc}\Big|_{c=\sqrt{2}/2}\cos(\gamma)\beta \tag{3.24}$$

Where $c = \cos(\theta)$. Working out the derivative of the associated Legendre polynomial from its definition results in the following

$$\frac{dP_l^m(c)}{dc} = \frac{1}{1-c^2}[(l+1)cP_l^m(c) - (l-m+1)P_{l+1}^m(c)] \tag{3.25}$$

$$\frac{dP_l^m(c)}{dc}\Big|_{c=\sqrt{2}/2} = \sqrt{2}(l+1)P_l^m(\sqrt{2}/2) - 2(l-m+1)P_{l+1}^m(\sqrt{2}/2) \tag{3.26}$$

We substitute our results: equations 3.19, 3.24 and 3.26 into the definition of the spherical harmonics, 3.8. For readability c_l^m is defined as

$$c_l^m = \sqrt{\frac{2l+1}{4\pi}\frac{(l-m)!}{(l+m)!}} \tag{3.27}$$

This gives

$$Y_l^m(\theta(\gamma,\Gamma),\phi(\gamma,\Gamma)) = \quad c_l^m e^{im(\gamma-\Gamma)}P_l^m(\sqrt{2}/2) + \tag{3.28}$$

$$c_l^m e^{im(\gamma-\Gamma)}P_l^m(\sqrt{2}/2)im\sin(\gamma)\beta + \tag{3.29}$$

$$c_l^m e^{im(\gamma-\Gamma)}\frac{dP_l^m(c)}{dc}\Big|_{c=\sqrt{2}/2}\sqrt{2}/2\cos(\gamma)\beta \tag{3.30}$$

Where a term is dropped, as working out the multiplication gives a $...\beta^2$ term and only the first order of β is considered. Filling 3.28 in the integral from equation 3.2 can be analytically calculated. This is done for all considered values of n, k, l, m and the matrix is given in table.

	M_0^0	M_1^{-1}	M_1^0	M_1^1	M_2^{-2}	M_2^{-1}	M_2^0	M_2^1	M_2^2	M_3^{-3}	M_3^{-2}	M_3^{-1}	M_3^0	M_3^1	M_3^2	M_3^3
f_{-2}^{-2}	0	0	0	0	0	0	0	0	0	0	0	0	0	0	0	0
f_{-1}^{-2}	0	0	0	0	0	0	0	0	0	0	0	0	0	0	0	0
f_{0}^{-2}	0	0	0	0	0	0	0	0	0	0	0	0	0	0	0	0
f_{1}^{-2}	0	0	0	0	0	0	0	0	0	0	$\frac{\sqrt{105}\beta}{32\sqrt{\pi}}$	0	0	0	$\frac{\sqrt{105}\beta}{32\sqrt{\pi}}$	0
f_{2}^{-2}	0	0	0	0	0	0	0	0	$\frac{\sqrt{30}}{16\sqrt{\pi}}$	0	0	0	0	0	$\frac{\sqrt{105}}{16\sqrt{\pi}}$	0
f_{-2}^{-1}	0	0	0	0	0	0	0	0	0	0	0	0	0	0	0	0
f_{-1}^{-1}	0	0	0	0	0	0	0	0	0	0	0	0	0	0	0	0
f_{0}^{-1}	0	0	0	0	0	$-\frac{\sqrt{30}\beta}{16\sqrt{\pi}}$	0	$\frac{\sqrt{30}\beta}{16\sqrt{\pi}}$	0	0	0	$-\frac{5\sqrt{42}\beta}{32\sqrt{\pi}}$	0	$\frac{5\sqrt{42}\beta}{32\sqrt{\pi}}$	0	0
f_{1}^{-1}	0	0	0	$\frac{\sqrt{3}}{4\sqrt{\pi}}$	0	0	0	$\frac{\sqrt{30}}{8\sqrt{\pi}}$	0	0	0	0	0	$\frac{3\sqrt{42}}{32\sqrt{\pi}}$	0	0
f_{2}^{-1}	0	$\frac{\sqrt{3}\beta}{4\sqrt{\pi}}$	0	$-\frac{\sqrt{3}\beta}{4\sqrt{\pi}}$	0	$\frac{\sqrt{30}\beta}{16\sqrt{\pi}}$	0	$-\frac{\sqrt{30}\beta}{16\sqrt{\pi}}$	0	0	0	$-\frac{\sqrt{42}\beta}{16\sqrt{\pi}}$	0	$\frac{\sqrt{42}\beta}{16\sqrt{\pi}}$	0	0
f_{-2}^{0}	0	0	0	0	0	0	0	0	0	0	0	0	0	0	0	0
f_{-1}^{0}	0	0	$\frac{\sqrt{6}\beta}{8\sqrt{\pi}}$	0	0	0	$\frac{3\sqrt{5}\beta}{8\sqrt{\pi}}$	0	0	0	0	0	$\frac{9\sqrt{14}\beta}{32\sqrt{\pi}}$	0	0	0
f_{0}^{0}	$\frac{1}{2\sqrt{\pi}}$	0	$\frac{\sqrt{6}}{4\sqrt{\pi}}$	0	0	0	$\frac{\sqrt{5}}{8\sqrt{\pi}}$	0	0	0	0	0	$-\frac{\sqrt{14}}{16\sqrt{\pi}}$	0	0	0
f_{1}^{0}	0	0	$\frac{\sqrt{6}\beta}{8\sqrt{\pi}}$	0	0	0	$\frac{3\sqrt{5}\beta}{8\sqrt{\pi}}$	0	0	0	0	0	$\frac{9\sqrt{14}\beta}{32\sqrt{\pi}}$	0	0	0
f_{2}^{0}	0	0	0	0	0	0	0	0	0	0	0	0	0	0	0	0
f_{-2}^{1}	0	0	0	0	0	0	0	0	0	0	0	0	0	0	0	0
f_{-1}^{1}	0	$-\frac{\sqrt{3}}{4\sqrt{\pi}}$	0	0	0	$-\frac{\sqrt{30}}{8\sqrt{\pi}}$	0	0	0	0	0	$-\frac{3\sqrt{42}}{32\sqrt{\pi}}$	0	0	0	0
f_{0}^{1}	0	0	0	0	0	0	0	0	0	0	0	0	0	0	0	0
f_{1}^{1}	0	0	0	0	0	0	0	0	0	0	0	0	0	0	0	0
f_{2}^{1}	0	0	0	0	0	0	0	0	0	0	0	0	0	0	0	0
f_{-2}^{2}	0	0	0	0	$\frac{\sqrt{30}}{16\sqrt{\pi}}$	0	0	0	0	0	$\frac{\sqrt{105}}{16\sqrt{\pi}}$	0	0	0	0	0
f_{-1}^{2}	0	0	0	0	0	0	0	0	0	0	0	0	0	0	0	0
f_{0}^{2}	0	0	0	0	0	0	0	0	0	0	0	0	0	0	0	0
f_{1}^{2}	0	0	0	0	0	0	0	0	0	0	0	0	0	0	0	0
f_{2}^{2}	0	0	0	0	0	0	0	0	0	0	0	0	0	0	0	0

Table 3.1: The transfer matrix for face-on observations, with $l_{max} = 3$, and $-2 \leq n, k \leq 2$. $\beta = \pi/10$.

3.3 Observing with edge-on orientation

Now, we consider the case of $I = 0$. This means the observer is in the plane of the orbit, the observation is edge-on. In chapter 1 we saw that the intensity of the reflected light depends on the location of the planet in the orbit, given by Eq. 1.5. This makes the integral 3.2 too complicated to compute analytically. Another problem with the edge-on case comes from the fact that the value of α has to be taken into account to calculate the transfer matrix.
In this sub chapter, Y_l^m, $\theta(\gamma, \Gamma)$ and $\phi(\gamma, \Gamma)$ for edge-on observations are worked out to give a better insight into the transfer matrix, mainly into the effect of α and β. The integral from Eq. 3.2 will be computed numerically As in the previous sub chapter, we start by working out θ, ϕ from the location of the glint, which is given as equation 1.18

$$\hat{s}(t) = \begin{pmatrix} \sin(\gamma/2) \\ -\cos(\gamma/2) \\ 0 \end{pmatrix} \sigma(\sin(\gamma/2)) \tag{3.31}$$

Where the relation between the reflection point $\hat{s}(t)$on the planet in the coordinate of the solar system and the reflection point $\hat{p}(t)$ in the reference frame of the rotating planet is given as follows

$$\hat{p}(t) = R_z(-(\Gamma - \alpha))R_y(-\beta)R_z(-\alpha)\hat{s}(t) \tag{3.32}$$

Where we correct for the offset from the axial tilt by substracting α. This is done because it leads to a simpler expression, and it is allowed because the $t = 0$ point for the daily rotation can be chosen arbitrarily.
Again, small values for β are assumed, so the Taylor expansion of $R_y(\beta)$ is taken, just as the face-on calculation. Working out the rotation matrices gives the following expression for $\hat{p}(t)$

$$\hat{p}(t) = \begin{pmatrix} -\sin(\Gamma - \gamma/2) \\ -\cos(\Gamma - \gamma/2) \\ -\beta\sin(\alpha - \gamma/2) \end{pmatrix} \sigma(\sin(\gamma/2) \tag{3.33}$$

We want to find the azimuth angle ϕ and the polar angle θ. To find the azimuth angle we look at the complex plane, with the x component on the real axis and the y component on the imaginary axis. In the expression for $\hat{p}(t)$ a sign function is present. This would give problems in working out the analytical expressions. But, realising we only consider $\gamma \in [0, 2\pi)$, the sign of $\sin(\gamma/2)$ is always positive, so the sign function can be ignored. This results in the following equations for ϕ and θ

$$e^{i\phi} = -\sin(\Gamma - \gamma/2) - i\cos(\Gamma - \gamma/2), \qquad \phi = \Gamma - \gamma/2 - \pi/2 \tag{3.34}$$

$$\cos(\theta) = -\beta\sin(\alpha - \gamma/2), \qquad \theta = \pi/2 + \beta\sin(\alpha - \gamma/2) \tag{3.35}$$

Where the Taylor expansion for the arccosine is used to calculate an explicit expression for θ. Now, we want to find $e^{im\phi}$ and $P_l^m(\cos(\theta)$ for the spherical harmonics.

$$e^{i\phi} = -\sin(\Gamma - \gamma/2) - i\cos(\Gamma - \gamma/2) = e^{i(\Gamma - \gamma/2 - \pi/2)} \tag{3.36}$$

$$e^{im\phi} = e^{im(\Gamma - \gamma/2 - \pi/2)} \tag{3.37}$$

For the Associated Legendre Polynomials we get

$$P_l^m(\cos(\theta)) = P_l^m(0) - \beta\sin(\alpha - \gamma/2)\frac{dP_l^m(c)}{dc}\Big|_{c=0} \tag{3.38}$$

Where $c = -\beta\sin(\alpha - \gamma/2)$. The derivative of the Associated Legendre Polynomial is calculated in equation 3.25. Filling in $c = 0$ results in

$$\frac{dP_l^m}{dc}\Big|_{c=0} = -(l - m + 1)P_{l+1}^m(0) \tag{3.39}$$

The results , equations 3.37, 3.38 and 3.39, are substituted into the definition of the spherical harmonics, 3.8. For readability c_l^m is defined as

$$c_l^m = \sqrt{\frac{(2l+1)}{4\pi}\frac{(l-m)!}{(l+m)!}} \tag{3.40}$$

This gives

$$Y_l^m(\theta(\gamma,\Gamma),\phi(\gamma,\Gamma)) = c_l^m e^{im(\Gamma-\gamma/2-\pi/2)} P_l^m(0) + (l-m+1) c_l^m e^{im(\Gamma-\gamma/2-\pi/2)} \sin(\alpha-\gamma/2) P_{l+1}^m(0)\beta \quad (3.41)$$

This equation for the spherical harmonics gives rise to two matrices, where the sum of those matrices is the transfer matrix. We have a matrix independent of the tilt, and a matrix purely dependent on α and β. This property might be useful in finding the tilt of a planet, which is assumed to be known in this paper. This matrix is calculated for $\alpha = \beta = 10$ degrees, shown in table 3.2. The transfer matrix only has nonzero values for $n = m$, which makes sense. If the parts containing Γ in equation 3.2 are isolated, we get

$$e^{i\Gamma(m-n)} \quad (3.42)$$

As there are no other parts dependent on Γ, we can isolate this in the double integral, and the only nonzero values in the transfer matrix are when $m = n$ for the n from f_n^k and the m from M_l^m. Looking back at the equation for a matrix element Eq. 3.2 we still need to account for the reflectivity R_e. This expression cannot be analytically worked out inside the integral so Python is used to numerically calculate the integral. The matrix elements for which the value is smaller than the element is set to zero.

	M_0^0	M_1^{-1}	M_1^0	M_1^1	M_2^{-2}	M_2^{-1}	M_2^0	M_2^1	M_2^2	M_3^{-3}	M_3^{-2}	M_3^{-1}	M_3^0	M_3^1	M_3^2	M_3^3
f_{-2}^{-2}	0	0	0	0	−0.0198	0	0	0	0	0	0.0001	0	0	0	0	0
f_{-2}^{-1}	0	0	0	0	−0.0271	0	0	0	0	0	−0.0012	0	0	0	0	0
f_{-2}^{0}	0	0	0	0	−0.0350	0	0	0	0	0	−0.0023	0	0	0	0	0
f_{-2}^{1}	0	0	0	0	−0.0465	0	0	0	0	0	−0.0088	0	0	0	0	0
f_{-2}^{2}	0	0	0	0	−0.0350	0	0	0	0	0	−0.0023	0	0	0	0	0
f_{-1}^{-2}	0	−0.0178	0	0	0	−0.0022	0	0	0	0	0	0.0166	0	0	0	0
f_{-1}^{-1}	0	−0.0151	0	0	0	−0.0023	0	0	0	0	0	0.0141	0	0	0	0
f_{-1}^{0}	0	−0.0099	0	0	0	−0.0034	0	0	0	0	0	0.0093	0	0	0	0
f_{-1}^{1}	0	0.0099	0	0	0	0.0034	0	0	0	0	0	−0.0093	0	0	0	0
f_{-1}^{2}	0	0.0151	0	0	0	0.0023	0	0	0	0	0	−0.0141	0	0	0	0
f_{0}^{-2}	0.0198	0	0.0006	0	0	0	−0.0222	0	0	0	0	0	−0.0013	0	0	0
f_{0}^{-1}	0.0255	0	0.0011	0	0	0	−0.0286	0	0	0	0	0	−0.0025	0	0	0
f_{0}^{0}	0.0339	0	0.0042	0	0	0	−0.0379	0	0	0	0	0	−0.0096	0	0	0
f_{0}^{1}	0.0255	0	0.0011	0	0	0	−0.0286	0	0	0	0	0	−0.0025	0	0	0
f_{0}^{2}	0.0198	0	0.0006	0	0	0	−0.0222	0	0	0	0	0	−0.0013	0	0	0
f_{1}^{-2}	0	0	0	−0.0151	0	0	0	−0.0023	0	0	0	0	0	0.0141	0	0
f_{1}^{-1}	0	0	0	−0.0099	0	0	0	−0.0034	0	0	0	0	0	0.0093	0	0
f_{1}^{0}	0	0	0	0.0099	0	0	0	0.0034	0	0	0	0	0	−0.0093	0	0
f_{1}^{1}	0	0	0	0.0151	0	0	0	0.0023	0	0	0	0	0	−0.0141	0	0
f_{1}^{2}	0	0	0	0.0178	0	0	0	0.0022	0	0	0	0	0	−0.0166	0	0
f_{2}^{-2}	0	0	0	0	0	0	0	0	−0.0350	0	0	0	0	0	−0.0023	0
f_{2}^{-1}	0	0	0	0	0	0	0	0	−0.0465	0	0	0	0	0	−0.0088	0
f_{2}^{0}	0	0	0	0	0	0	0	0	−0.0350	0	0	0	0	0	−0.0023	0
f_{2}^{1}	0	0	0	0	0	0	0	0	−0.0271	0	0	0	0	0	−0.0012	0
f_{2}^{2}	0	0	0	0	0	0	0	0	−0.0198	0	0	0	0	0	0.0001	0

Table 3.2: The transfer matrix for Edge-On observations, with $l_{max} = 3$, and $-2 \leq n, k \leq 2$. $\alpha = \beta = \pi/10$.

Chapter 4

Map Retrieval

We started this report by calculating the location of the glint on a planet for multiple orientations. A few algorithms were explained to construct a realistic random map. Then the theory behind spherical harmonics on spheres was explained. This was followed by calculating the light signal from reflections on water. Finally, we went into calculating the transfer matrix, which transforms a map vector of spherical harmonics into a vector of Fourier coefficients. This chapter solves the inverse problem.
In this chapter, we combine the knowledge and skills from all the previous chapters to retrieve ocean maps. The theory developed in this chapter will be applied to a planet generated using the great-circle algorithm from chapter 2.2.3. Furthermore, we assume the orientation of our measurements and the exoplanet is known, so the inclination I and the rotation axes (α, β) are known.

4.1 The pseudoinverse

In the previous chapter we introduced the transfer matrix. This matrix gives a linear transformation from an ocean map of an exoplanet to the light signal of the reflection directed towards Earth. An observer on Earth receives this light signal, and we would like to find the the ocean map from this signal. We could try $\mathbf{M} = A^{-1}\mathbf{f}$, where A^{-1} is the inverse of A. But in general, the inverse of the transfer matrix is not defined as the transfer function is not injective. There exists an alternative to the normal inverse, the **Moore-Penrose (pseudo)inverse** is a generalization of the inverse of a non-singular matrix, which exists for any matrix with complex elements. Let A the transfer matrix. Any map vector $\mathbf{M}$ can be decomposed to a projection on the row space of A and the null space of A. Let $\mathbf{M_n}$ the projection of $\mathbf{M}$ on the null space and let $\mathbf{M_r}$ denote the projection of $\mathbf{M}$ on the row space. Because the vector $\mathbf{M_n}$ maps to the null space, we get $A\mathbf{M_n} = \mathbf{0}$. And if $Null(A)$ contains nonzero vectors, we cannot recover the component $\mathbf{M_n}$ from a given $\mathbf{f}$. This also implies $\mathbf{M_r}$ is mapped to the same vector of Fourier coefficients $\mathbf{f}$ as $\mathbf{M}$. This null space can be physically understood by thinking about the measurement we are doing. We look at the light signal of the reflection on water that is directed towards Earth. In chapter 1.4 we went into the glint location on the exoplanet and we saw that the location of the glint moves inside a certain band. We do not expect a body of water outside of this band to influence the measured light signal, as light hitting this body of water is not reflected towards the observer. From the matrix in chapter 3, we can compute the null space, and we see that it contains nonzero vectors. This means the inverse of the transfer matrix does not exist. So we use the Moore-Penrose pseudoinverse which is defined such that the following holds

$$A^+ f = \begin{cases} \mathbf{M_r} & \text{if there exists an } \mathbf{M_r} \in Row(A) \text{ such that } A\mathbf{M_r} = \mathbf{f} \\ \mathbf{0} & \text{if } \mathbf{f} \in Null(A^T) \end{cases} \tag{4.1}$$

Where A^+ is the pseudoinverse. $\mathbf{M_r}$ is the projection of $\mathbf{M}$ on the row space of A and $\mathbf{f}$ is the vector of Fourier coefficients where we assumed $\mathbf{f} = A\mathbf{M}$ holds. Eq. 4.1 does not help us compute the pseudoinverse, but it gives some insight into the properties of the pseudoinverse.

4.2 The Singular Value Decomposition

The pseudoinverse of A is related to the singular value decomposition (SVD) of A. This relation is a generalization of the spectral decompositions for non-square matrices. The SVD is a factorization of a

matrix A, we can write any matrix A as the product of three matrices:

$$A = U\Sigma V^T \tag{4.2}$$

Where U and V are real orthogonal matrices. Σ is a diagonal matrix, the diagonal entries are the singular values of A. The SVD has a few useful applications. The range, null space and rank of A can be found from the SVD. The number of nonzero singular values is equal to the rank of the matrix A. The SVD also provides an explicit representation of the range and null space of a matrix. Let n the total number of singular values of A with r the rank of the matrix. The null space is spanned by the last $n - r$ rows of V^T, while the range is spanned by the first r rows of U.
The most important application of the SVD is that it can be used for computing the pseudoinverse of a matrix. The pseudoinverse of matrix A with singular value decomposition $A = U\Sigma V^T$ is

$$A^+ = V\Sigma^+ U^T \quad \sum_{k=1}^{r} \frac{1}{\sigma_k} \mathbf{v}_k \mathbf{u}_k^T \tag{4.3}$$

Where Σ^+ is a diagonal matrix with, for the nonzero singular values, the inverse of the singular values on the diagonal, and 0 if the singular value is zero.

4.3 Map retrieval using the pseudoinverse

In chapter 2 we described a way to represent a surface map as a vector of spherical harmonic coefficients. Plotting a surface map from this vector can be done as follows

$$M(\theta, \phi) = \sum_{l=0}^{\infty} \sum_{m=-l}^{l} M_l^m Y_l^m(\theta, \phi) \tag{4.4}$$

If we have a vector of Fourier coefficients, using the pseudoinverse, we can obtain an approximation of the original map. Multiplying the pseudoinverse with the vector $\mathbf{f}$ gives the projection of M on the row space, $\mathbf{M_r}$. Intuitively, this gives the best obtainable approximation for $\mathbf{M}$ from the limited information we receive. The problem then becomes finding $\mathbf{f}$ In this report, two possible ways to find the vector of Fourier coefficients are explored. In theory, the vector of Fourier coefficients is simply given by $\mathbf{f} = A\mathbf{M}$. The vector of Fourier coefficients can be calculated from measuring the light signal. To reconstruct a measurement we use a map generated using the Great-Circle Algorithm described in chapter 2.2.3, fig 2.4. From this map we can calculate the map vector $\mathbf{M}$. We assume the tilt axes are known, meaning the transfer matrix A is known. Using eq. 3.3, we calculate $\mathbf{f}$. We can also directly calculate the vector $\mathbf{f}$ by integrating over time. Again, we apply our theory on the map from fig 2.4. This time we calculate the vector of Fourier coefficients by measuring the light signal. To evaluate the integral from eq. 3.2 we need to be able to vary the day and year angle independently, Γ and γ respectively. To do this, two assumptions have to be made, the measurement is done continuously and infinitely long and Γ/γ is irrational. Both these assumptions are very strict. We use these assumptions to describe the theory. In practice, the closer we get to these conditions, the better the map retrieval. Going back to integral 3.2, being able to vary Γ and γ independently gives a rather straightforward way to calculate $\mathbf{f}$ by transforming the integral into a sum.
With the pseudoinverse we are now ready to test the retrieval.

4.3.1 Face-On retrieval

For an Face-On observation with $\beta = \pi/10$ our retrieval looks as in figure 4.1. Figure 4.1a shows the map the theory is tested on. The water is plotted in white, black is surface for which we assumed it does not reflect light. The red lines show the band in which the glint moves. Figure 4.1b shows the same map, limiting the number of spherical harmonics used to construct the map. This map shows more accurately what we will retrieve, as the transfer matrix only takes these spherical harmonics into account, with $l_{max} = 4$. The third map shows the retrieval where $\mathbf{f}$ is calculated from Eq. 3.3. Fig 4.1d shows the retrieval where the vector of Fourier coefficients is directly calculated from the map. We see that a lot of information outside of the band in which the glint moves is accurately retrieved. This may be due to numerical inaccuracies in the calculation which get amplified in the pseudo-inverse. AWe see that the map is partially retrieved outside of the band in which the glint moves. This could be explained by the

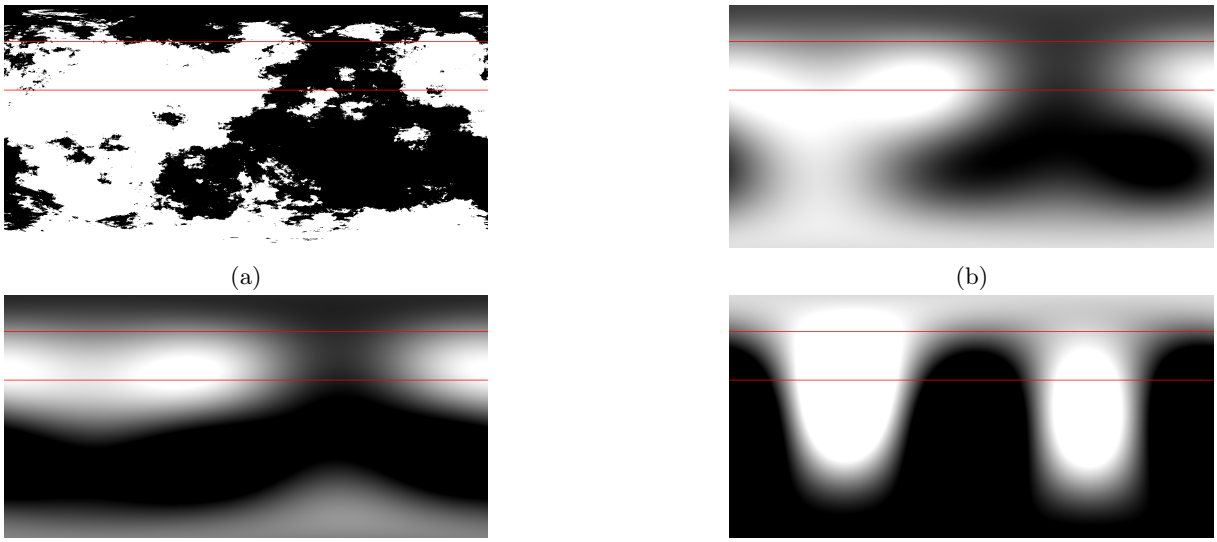

(a) (b) (c) (d)

Figure 4.1: Retrieval for Face-On observation of the map 4.1a for β known, $\beta = \pi/10$. The red lines are drawn to mark the band in which the glint moves. Fig 4.1a shows the original map attempted to retrieve, fig 4.1b shows the resolution of the retrieval, $l_{max} = 4$, chapter 2 further goes into this choice. Here $n_{max} = k_{max} = 3$ is chosenfor the Fourier coefficients. The resolution also affects the size of the matrix from chapter 3. Fig 4.1c is plotted using Eq. 3.3 to calculate the vector of Fourier coefficients $\mathbf{f}$, while fig 4.1d is created by directly measuring the light signal. The rank of the transfer matrix A is 10.

fact that the spherical harmonics are not precisely defined in the band, so while the presence of a certain spherical harmonic is only measured inside the band, the actual spherical harmonic also contributes to the map outside of the band. For figure 4.1d we see two big white spots. This could be due to numerical error plotting a vector from the null space.

4.3.2 Edge-On retrieval

For an Edge-On observation with $\alpha = \beta = \pi/10$ our retrieval looks as in figure 4.2. Figure 4.2a shows the map the theory is tested on. The water is plotted in white, black is surface for which we assumed it does not reflect light. The red lines show the band in which the glint moves. Figure 4.2b shows the same map, limiting the number of spherical harmonics used to construct the map. This map shows more accurately what we will retrieve, as the transfer matrix only takes these spherical harmonics into account, with $l_{max} = 4$. The third map shows the retrieval where $\mathbf{f}$ is calculated from Eq. 3.3. Fig 4.2d shows the retrieval where the vector of Fourier coefficients is directly calculated from the map. The two methods to calculate $\mathbf{f}$, described before, should be the same calculation, but the retrieval is a bit different. Still, the shapes in the band are pretty close to the map we try to retrieve. The difference in these maps could be explained by small rounding errors in the numerical calculations needed for the transfer matrix in the case of Edge-On observations. We see that the map is partially retrieved outside of the band in which the glint moves. This could be explained by the fact that the spherical harmonics are not precisely defined in the band, so while the presence of a certain spherical harmonic is only measured inside the band, the actual spherical harmonic also contributes to the map outside of the band.

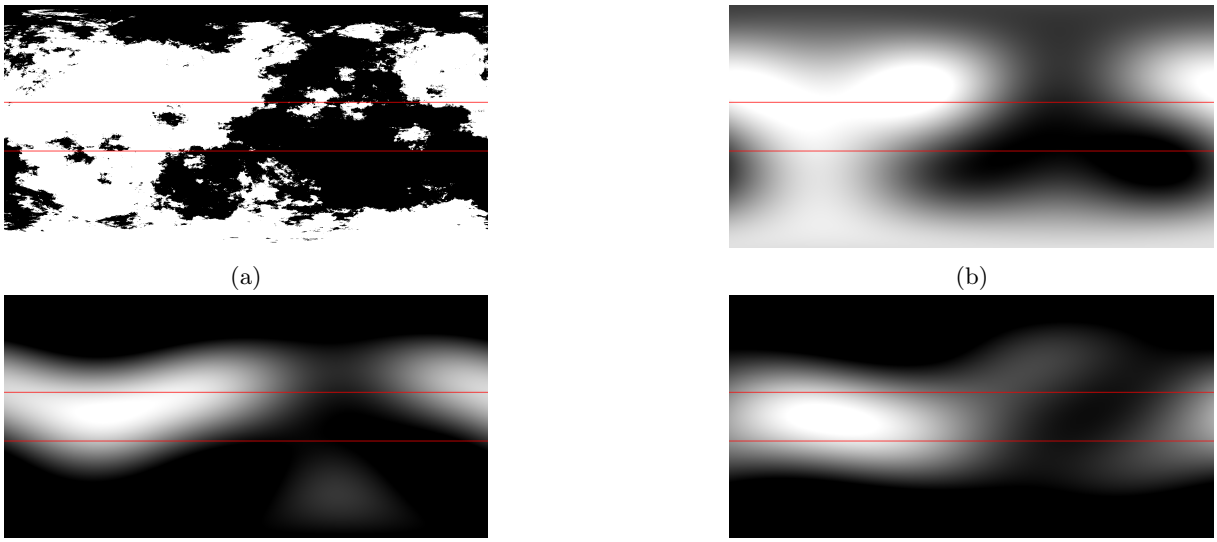

(a) (b)

(c) (d)

Figure 4.2: Retrieval for Edge-On observation of the map 4.2a for α and β known, $\alpha = \beta = \pi/10$. The red lines are drawn to mark the band in which the glint moves. Fig 4.2a shows the original map attempted to retrieve, fig 4.2b shows the resolution of the retrieval, $l_{max} = 3$, chapter 2 further goes into this choice. Here $n_{max} = k_{max} = 2$ is chosen for the Fourier coefficients. The resolution also affects the size of the matrix from chapter 3. Fig 4.2c is plotted using Eq. 3.3 to calculate the vector of Fourier coefficients $\mathbf{f}$, while fig 4.2d is created by directly measuring the light signal. The rank of A is 11.

Chapter 5

Discussion and Conclusion

The aim of this research was to explore a new variation of Spin-Orbit Tomography (SOT). Instead of splitting a surface map into finite sized pixels, the surface map was constructed using spherical harmonics. The time signal was decomposed into its freqency components. The first chapter went into the properties of the light curve and the information which could be deduced from measurements. The second chapter went into spherical harmonics and how they were used in this report. The third chapter we explored the relation between a surface map and the measured light signal. We did this by finding a linear transformation between the surface map, constructed from spherical harmonics and the time signal, decomposed into Fourier coefficients, this linear transformation was defined by the transfer matrix. The final chapter went into map retrieval, by finding a pseudo inverse of the transfer matrix a map could partially be constructed from a light signal.

In chapter 1 we looked into Fresnel reflection of light. For light reflecting on water, the incoming angle is the same as the outgoing angle. This means the light reflected off the surface of a planet comes from a point source on the planet, we called the location of this point source the glint location. Due to the orientation of a solar system with respect to the observer we have shown that the glint location moves in a band on the planet, where the size of the band depends on the tilt axis. In this chapter two different orientations were explored, the face-on observation and the edge-on observation. For face-on observations, the intensity of the reflected light was constant, for edge-on observation, the intensity was not constant. This later allows for analytical calculations for face-on observation. However, for edge-on observation, the light curve contains more information because of this which improved the retrieval. In chapter 2 we have seen that we can roughly reconstruct a map from a limited number of spherical harmonics. In chapter 3 we saw that we can decompose a light signal into a basis of complex exponentials. Eq. 2.1 and 3.1

$$M(\theta,\phi) = \sum_{l=0}^{\infty}\sum_{m=-l}^{l} M_l^m Y_l^m(\theta,\phi) \qquad \approx \sum_{l=0}^{l_{max}}\sum_{m=-l}^{l} M_l^m Y_l^m(\theta,\phi)$$

$$f(\gamma,\Gamma) = \sum_{k=-\infty}^{\infty}\sum_{l=-\infty}^{\infty} f_k^n e^{i(k\gamma+n\Gamma)} \qquad \approx \sum_{k=-k_{max}}^{k_{max}}\sum_{n=-n_{max}}^{n_{max}} f_k^n e^{i(k\gamma+n\Gamma)}$$

The approximations are necessary for practical reasons. l_{max} determines the number of spherical harmonics taken into account, which affects the sharpness of the map. k_{max} determines the amount of detail with which the annual rotation can be observed. n_{max} determines the amount of detail with which the diurnal rotation can be observed. Chapter 3 also introduced the transfer matrix. The transfer matrix is a linear transformation which relates the outputs of the system to its inputs. In this case, the system is the light reflection, the input is the ocean map of a planet, and the output is the light signal of the reflection that is directed towards Earth. Eq. 3.3

$$\mathbf{f} = A(I,\alpha,\beta)\mathbf{M} \tag{5.1}$$

Where $\mathbf{f}$ is a vector of Fourier coefficients and $\mathbf{M}$ is a vector of spherical harmonics, the map vector. The transfer matrix is denoted by A. An element of the transfer matrix can be found by working out the following integral, Eq. 3.2

$$a_{i,j} = \int_0^{2\pi}\int_0^{2\pi} e^{-i(k\gamma+n\Gamma)} R_e(\gamma) Y_l^m(\theta(\gamma,\Gamma),\phi(\gamma,\Gamma)) d\gamma d\Gamma$$

Where $R_e(\gamma)$ appears as we have found in chapter 1 that the intensity of the reflected light depends on the diurnal angle γ. We find that the transfer matrix is purely dependent on the incliation I and the axial tilt described by α, β. For the case of face-on observations, we saw that the transfer matrix can be expressed purely in analytical terms, where we have used a few small angle approximations. Due to the complexity of $R_e(\gamma)$ for edge-on observations, the transfer matrix could only be expressed numerically. In chapter 4 we see that the nullspace of the transfer matrix contains nonzero vectors. This means that the inverse of the transfer matrix does not exist. So we use the Moore-Penrose pseudoinverse. Because of this, when attempting to retrieve a surface map, a certain part of the map is in the null space of A and it cannot be retrieved. This loss of information can be understood by thinking back to chapter 1 and realising the glint moved in a band. The surface outside of the band is never hit by a ray of light that can be reflected towards the observer, so information of the surface outside the band never reaches the observer.

Further research

Further research into this subject may be conducted in two areas.

At the start of the report we assumed the axial tilt was known. However, the tilt is not something that can easily be measured. An analysis on the column space could give the axial tilt. Van Oosterom [2019] came to the conclusion that $Col(A(\alpha, \beta))$ was independent of the values of α and β for Lambertian reflection. Perhaps Fresnel reflection is not. Van Oosterom [2019] attempted to find the axial tilt using Tikhonov Regularization and by minimizing α and β for negative values in the retrieved surface map. Van Oosterom [2019] proved unsuccesful, perhaps this changes for Fresnel reflections.

This report only looked at face-on and edge-on observations. These exact orientations are not expected in real measurements. The same calculations could be done without specifying the value for the inclination I to have a more realistic way to retrieve surface maps.

Bibliography

N. B. Cowan and E. Agol. Inverting Phase Functions to Map Exoplanets. *The Astrophysical Journal*, 678(2):L129–L132, 2008. doi: 10.1086/588553.

Y. Fujii and H. Kawahara. MAPPING EARTH ANALOGS FROM PHOTOMETRIC VARIABILITY: SPIN-ORBIT TOMOGRAPHY FOR PLANETS IN INCLINED ORBITS. *The Astrophysical Journal*, 755(2):101, 2012. doi: 10.1088/0004-637x/755/2/101.

Y. Fujii, H. Kawahara, Y. Suto, A. Taruya, S. Fukuda, T. Nakajima, and E. L. Turner. COLORS OF A SECOND EARTH: ESTIMATING THE FRACTIONAL AREAS OF OCEAN, LAND, AND VEGETATION OF EARTH-LIKE EXOPLANETS. *The Astrophysical Journal*, 715(2):866–880, 2010. doi: 10.1088/0004-637x/715/2/866.

Y. Fujii, H. Kawahara, Y. Suto, S. Fukuda, T. Nakajima, T. A. Livengood, and E. L. Turner. COLORS OF A SECOND EARTH. II. EFFECTS OF CLOUDS ON PHOTOMETRIC CHARACTERIZATION OF EARTH-LIKE EXOPLANETS. *The Astrophysical Journal*, 738(2):184, 2011. doi: 10.1088/0004-637x/738/2/184.

LBTO. Large Binocular Telescope Observatory, 2020. URL `https://www.lbto.org/`.

NASA. Exoplanet Exploration, Planets Beyond Our Solar System, 09 2021. URL `https://exoplanets.nasa.gov/`.

S. Van Oosterom. *Exoplanet surface mapping.* Bachelor thesis, TU Delft, 2019.

Wikipedia contributors. List of nearest exoplanets, 08 2021. URL `https://en.wikipedia.org/wiki/List_of_nearest_exoplanets`.

Appendix A

Additional recovered maps for edge-on observation

The retrieval is tried for multiple planet maps and varying values of l_{max} and $n_{max} = k_{max}$ and for different values of α and β. The retrieval can be found on the next page, plotted the same way as in chapter 4.

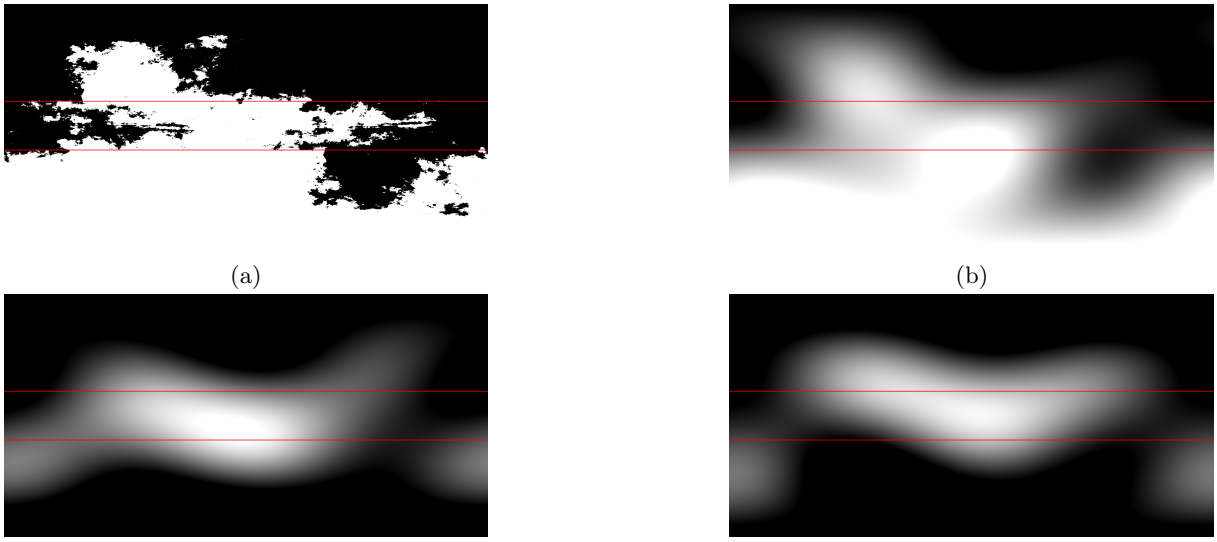

(a) (b)

(c) (d)

Figure A.1: Retrieval for Edge-On observation of the map A.1a for α and β known, $\alpha = \beta = \pi/10$. The red lines are drawn to mark the band in which the glint moves. Fig A.1a shows the original map attempted to retrieve, fig A.1b shows the resolution of the retrieval, $l_{max} = 4$, chapter 2 further goes into this choice. Here $n_{max} = k_{max} = 2$ is choesen for the Fourier coefficients. The resolution also affects the size of the matrix from chapter 3. Fig A.1c is plotted using Eq. 3.3 to calculate the vector of Fourier coefficients $\mathbf{f}$, while fig A.1d is created by directly measuring the light signal.

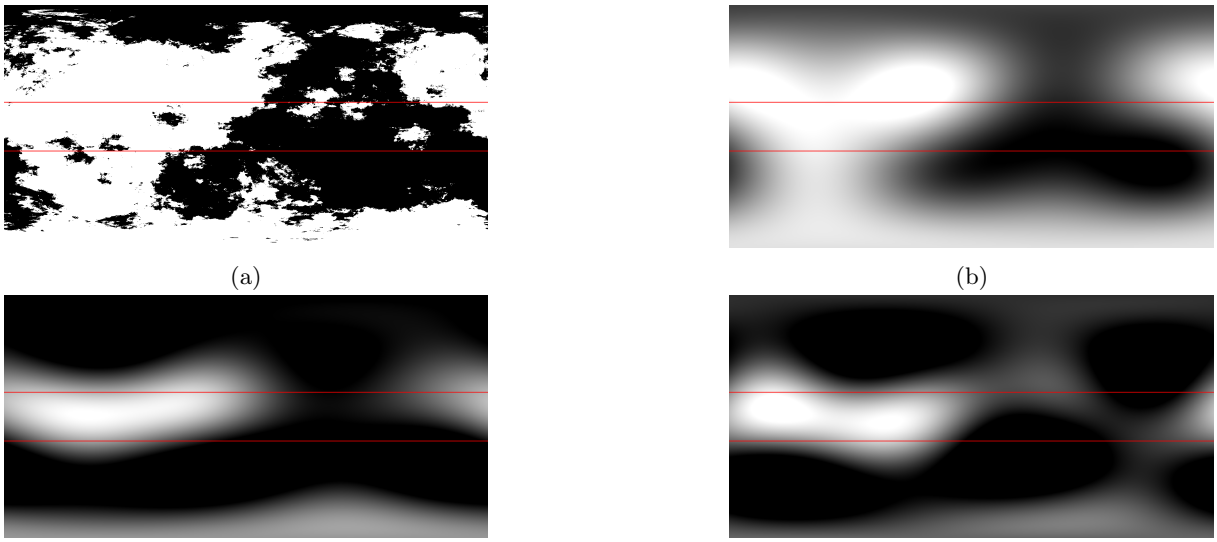

(a) (b)

(c) (d)

Figure A.2: Retrieval for Edge-On observation of the map A.2a for α and β known, $\alpha = \beta = \pi/10$. The red lines are drawn to mark the band in which the glint moves. Fig A.2a shows the original map attempted to retrieve, fig A.2b shows the resolution of the retrieval, $l_{max} = 4$, chapter 2 further goes into this choice. Here $n_{max} = k_{max} = 3$ is chosen for the Fourier coefficients. The resolution also affects the size of the matrix from chapter 3. Fig A.2c is plotted using Eq. 3.3 to calculate the vector of Fourier coefficients $\mathbf{f}$, while fig A.2d is created by directly measuring the light signal. The rank of A is 16.

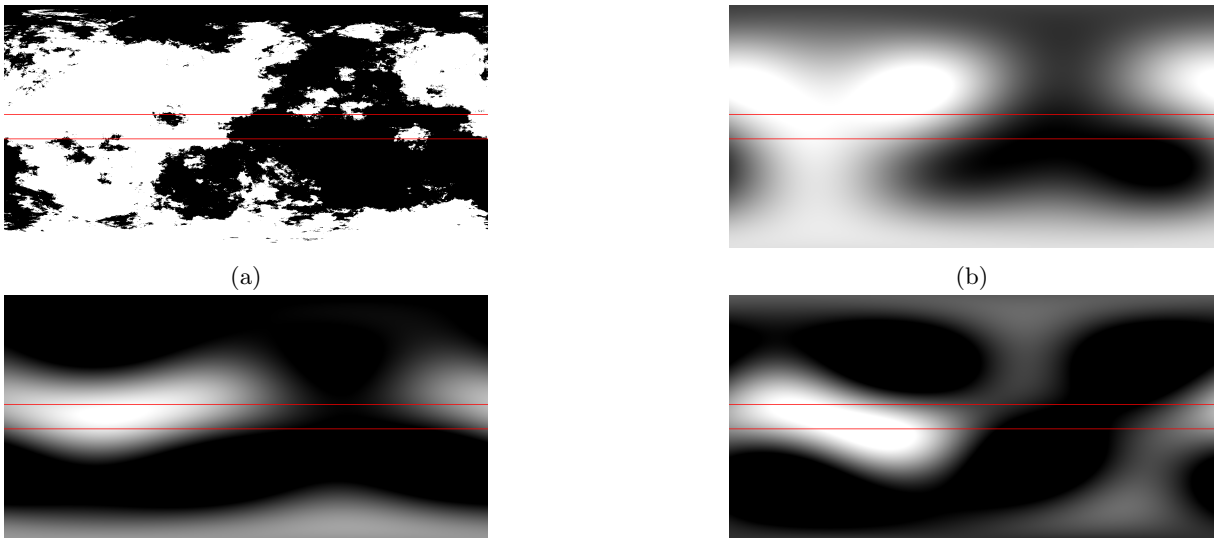

(a) (b)

(c) (d)

Figure A.3: Retrieval for Edge-On observation of the map A.3a for α and β known, $\alpha = \beta = \pi/20$. The red lines are drawn to mark the band in which the glint moves. Fig A.3a shows the original map attempted to retrieve, fig A.3b shows the resolution of the retrieval, $l_{max} = 3$, chapter 2 further goes into this choice. Here $n_{max} = k_{max} = 3$ is chosen for the Fourier coefficients. The resolution also affects the size of the matrix from chapter 3. Fig A.3c is plotted using Eq. 3.3 to calculate the vector of Fourier coefficients $\mathbf{f}$, while fig A.3d is created by directly measuring the light signal. The rank of A is 11.

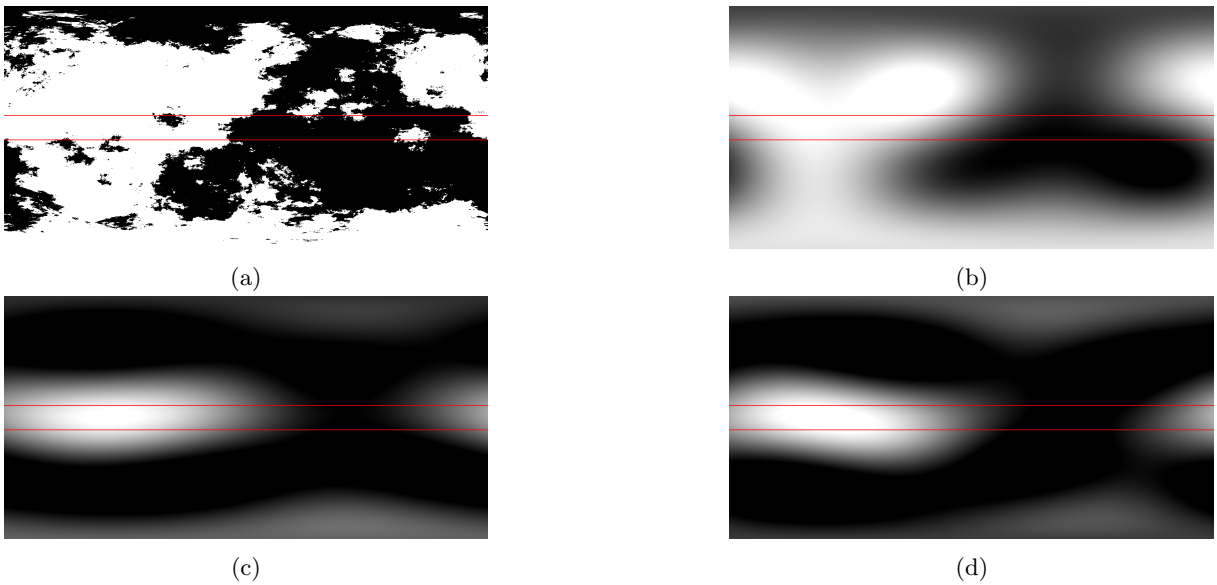

(a) (b)

(c) (d)

Figure A.4: Retrieval for Edge-On observation of the map A.4a for α and β known, $\alpha = \beta = \pi/20$. The red lines are drawn to mark the band in which the glint moves. Fig A.3a shows the original map attempted to retrieve. For this retrieval, the pseudo-inverse is calculated with the wrong values of α and β, namely $\alpha = \beta = \pi/10$, fig A.4b shows the resolution of the retrieval, $l_{max} = 4$, chapter 2 further goes into this choice. Here $n_{max} = k_{max} = 3$ is chosen for the Fourier coefficients. The resolution also affects the size of the matrix from chapter 3. Fig A.4c is plotted using Eq. 3.3 to calculate the vector of Fourier coefficients $\mathbf{f}$, while fig A.4d is created by directly measuring the light signal. The rank of A is 15.

Appendix B

Code

All of the code that has been used in this report is available on request at:
T.Mulder@student.tudelft.nl